Heliyon 9 (2023) e14225

Contents lists available at ScienceDirect

Heliyon

journal homepage: www.cell.com/heliyon

Review article

A state-of-the-art review on experimental investigation and finite element analysis on structural behaviour of fibre reinforced polymer reinforced concrete beams

B.A. Solahuddin *, F.M. Yahaya

Faculty of Civil Engineering Technology, Level 1, Chancellery Building, Universiti Malaysia Pahang, Lebuh Persiaran Tun Khalil Yaakob, 26300 Kuantan, Pahang Darul Makmur, Malaysia

A R T I C L E I N F O

Keywords:
Fibre reinforced polymer
Reinforced concrete beams
Structural behaviour
Load-deflection
Ultimate load
Stiffness
Energy absorption
Experimental investigation
Finite element analysis
Numerical modelling

A B S T R A C T

Fibre reinforced polymer (FRP) composite is a useful material. It has been utilised to enhance the structural behaviour of reinforced concrete beams (RCB). It is also crucial to summarise the impact of FRP on various types of RCB properties. This study summarises the FRP usage's impact on the RCB's structural behaviour based on previous research by reviewing and discussing the experimental study and finite element analysis (FEA) results. Based on previous relevant literature reviews, the experimental investigation and FEA showed significant improvements in flexure, stiffness, young modulus, load-deflection, ultimate load capacity, fracture pattern, and failure mode when FRP was used in RCB production. This FRP composite material can be used as the external reinforcement for RCB due to its high strength capability, force, load, and corrosion resistance with adhesive and anchorage properties. Using FRP in RCB can benefit civil engineering by increasing its structural behaviour and performance, especially in construction industry.

1. Introduction

FRP is synthetic, natural and hybrid fibre composite material as an alternative for RCB wrapping. FRP contains high-fibre properties incorporated in polymer matrices [1]. The fibres are strong, durable and impervious to harm from any other elements available in the mixture [2]. Fibres are one of the main reinforcement parts because the polymer matrices act as a binder to shield the fibres and also transmit stress between them [3]. Additionally, they also have a long fatigue life and structural plasticity [4]. There are many types of fibres, such as natural, synthetic, and hybrid fibres. Jute, kenaf, and cellulose are natural fibres [1]. Glass, carbon, aramid and kevlar are synthetic fibres, while sisal/glass and jute/glass are hybrid fibres [1]. All these three types of fibres are predominantly used to develop new composite materials [1]. Lightweight, high strength, and great corrosion resistance are a few characteristics of FRP composite. These characteristics meet all of the requirements mentioned above as the strengthening method.

Reinforced concrete beams, slabs, joints, and frames can be constructed in various shapes, such as rectangular, square, and circular. They could be reinforced with either E-glass-epoxy or carbon-epoxy. FRP composite was utilised as the external reinforcement for beam-column joints in conventional building construction in the late 1990s [5]. A common technique for using FRP in reinforced concrete construction is by wrapping it either at a particular section or an entire surface [6–9]. The steel jacket application technology

* Corresponding Author.
E-mail address: solahuddin.08@yahoo.com (B.A. Solahuddin).

https://doi.org/10.1016/j.heliyon.2023.e14225
Received 17 November 2022; Received in revised form 6 February 2023; Accepted 26 February 2023
Available online 2 March 2023

was first used same as CFRP wrapping technique [10]. Concrete and reinforced concrete structures are wrapped with FRP as external reinforcement to increase structural behaviour and performance. Different FRP wrapping techniques, like hand layup [11] and carbon anchor [6], are available. Fig. 1 depicts the strengthening process of building structural components using FRP. This review will evaluate and discuss the strengthening of RCB with FRP composite material. The strength of new reinforced concrete (RC) structure reinforced by FRP will be summarised to acquire the best potential of the fibre material. Moreover, the relevance and the technologies used to wrap RCB with FRP composite material will be explored in this study by experimental investigation and finite element analysis (FEA). The FEA is utilised to simulate and analyse the experimental results.

One of the major causes of concrete structure deterioration is the corrosion of steel reinforcement. An alternative approach to addressing the corrosion problem in concrete structures is to use FRP reinforcement instead of steel reinforcement [12,13]. FRP reinforcement shows potential structural behaviour because of its low magnetic susceptibility, high strength-to-weight ratio, and resilience to corrosion. Carbon fibre reinforced polymer (CFRP) reinforcement is preferred to be used as prestressing tendons due to its high tensile strength and favourable creep resistance [14]. Glass fibre reinforced polymer (GFRP) reinforcement is commonly used as a non-prestressed bar in concrete structures due to its lower cost.

In the 1970s, scientists first began studying the effects of FRP reinforcement in prestressed concrete (PC) buildings. The flexural behaviour of FRP-PC components has been studied extensively over the past five decades, and the flexural design methodologies are well established [14–16]. However, FRP-PC beams' shear behaviour is not understood as well. FRP-PC beams without stirrups also fail in shear, but for the same reasons as steel-PC beams [17–21]: diagonal tension, shear compression, and inclined compression. All T-beams tested by Nabipay and Svecova [17] failed during shear compression, regardless of whether the shear span-to-effective depth ratio was 1.5, 2.5, or 3.5. A beam with a/d value between 1.41 and 2.14 failed in shear compression, and a beam with a/d of 0.71 failed in inclined compression, as determined by Wang et al. [18]. Moreover, FRP-PC beams without stirrups exhibited a novel diagonal tension failure initiated by rupture of the prestressed FRP tendon due to dowel action [19–21]. Recent shear tests on FRP-PC beams demonstrated that increasing the prestressing level or decreasing the shear span-to-effective depth ratio boosted the shear strength [22,23].

Complexity prevents a purely theoretical determination of PC beam shear strength [24]. The available semi-empirical approach is used to account for the parameters that affect the shear strength. There are several factors to consider, such as the amount and kind of flexural reinforcement, the concrete strength, the amount of pre-stressing, the ratio of shear span to effective depth, the member depth, etc. However, little attention is given to the variables that affect the shear strength of the FRP-PC beam. Much research on pre-tensioned concrete beams with an effective depth of 400 mm or less has been done so far. However, research is not devoted to post-tensioned concrete beams and columns of significant size. Current shear strength design formulas for FRP-PC members often lead to cautious predictions [22,25] and are primarily attributable to the scarcity of experimental investigation. For shear design approaches of FRP-PC beam, new research is still needed for full-scale members.

2. Fibre reinforced polymer

In 1940s, FRP composites were used in military and aerospace industries. This material usage and its applications have been used in a wide range. Several fibre reinforced polymer reinforced concrete (FRPRC) constructions have been constructed, such as roofs, walls, steel and PVS pipes, and many more. These FRPRC constructions of FRP pieces combined to form structural rigidity components. Polymer composites have been used extensively in the building industry over the past decade. Their usage has expanded, including bridge maintenance and design, structural cables, structural reinforcement, and also becoming a part of building components. These advanced composites have improved their characteristics and properties. Polymers reinforced with high strength, high modulus glass fibres and carbon are stuck in layers to form a new composite material. However, as the specification does not specify any particular material combination, it is vague. The basic of FRP materials and how researchers and civil engineers emphasise how they use FRP (Fig. 2) to reinforce and strengthen reinforced concrete beam is discussed in this review paper.

Even though paper, wood, and asbestos have occasionally been utilised, glass, carbon, and basalt are the most common fibres used

Fig. 1. Strengthening process of building structural components using FRP [11].

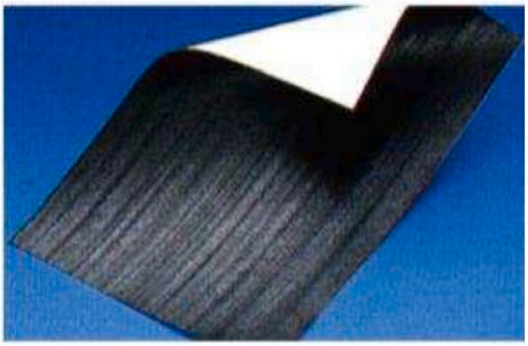

Fig. 2. Fibre reinforced polymer (FRP).

nowadays. Epoxy, vinyl ester, and polyester are typical examples of thermosetting polymers, but phenol-formaldehyde resins are still used. FRP is widely utilised in aviation, automobile, marine, and building construction. The fibre phase of composite materials is spread in a continuous matrix phase, making up the material as a whole. The fibres can be bonded to the polymer matrix in a particular position, direction, and volume at high-stress regions to get the highest reinforcement. The reinforcement could become a minimum of low-stress value within the homogenous member. As a bonus, the material is more efficient in construction and has several other benefits, including reducing weight and increasing corrosion resistance, durability, transparency, and carbon footprint. Fig. 3 shows the magnified FRP cross-section, showing an FRP strip with a thickness of around 0.8 mm in one direction located in the upper middle of the same strip. The depicted fibres have a diameter of about 5 mm, while the longitudinal strength of the strip is 3300 MPa [26].

3. Experimental investigation of fibre reinforced polymer reinforced concrete beams

This section discusses a state-of-the-art review of experimental investigations on the fibre reinforced polymer reinforced concrete beams (FRPRCB)'s structural behaviour.

3.1. (Chin et al., 2011) [27]

Table 1 shows the beam specimen specifications utilised in this research. Three specimens were investigated, such as control beam (CB), beams strengthening with FRP with circular (C-cfrp-f) and square (S-cfrp-f) openings, as shown in Fig. 4(a) and (b). Both circular and square openings with FRP showed an increase in the beam strength. The ultimate loads (Pu) for CB, C-cfrp-f, and S-cfrp-f were 115.67 kN, 164.4 kN, 86.07 kN. C-cfrp-f shows the highest Pu compared to CB and S-cfrp-f. The huge square hole increased the flexural strength more than the large circular hole. This is because the beam with circular opening including FRP contained fibre contents from the FRP properties. There was a 42% increase in strength compared to the CB's ultimate load. The load-deflection behaviour of C-cfrp-f and Scfrp-f followed the same pattern of stiffness as CB as shown in Fig. 7. C-cfrp-f exhibited higher ductility in the post-yielding stage than S-cfrp-f. The FRP was used to reinforce the beams. The beam flexural cracks were developed at the tension zone and outside of the restricted area when FRP was used as external reinforcement. As the fracture width increased, the diagonal cracks occurred at the middle span due to the beam failure occurred. When the diagonal cracks were formed, the bottom reinforcement was yielded, and the concrete near the support crushed suddenly, causing a shear failure, as depicted in Fig. 5. The diagonal split was around 15 mm wide.

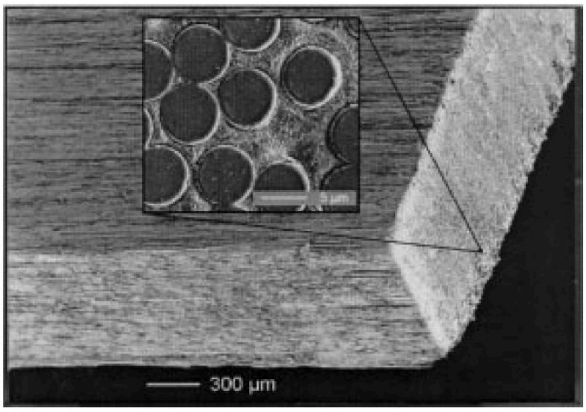

Fig. 3. Magnified FRP [26].

Table 1
Beam specimen details [27].

Beam	Opening	State
CB (Control)	None	No FRP laminates
C-cfrp-f	Circular	Have FRP laminates
S-cfrp-f	Square	Have FRP laminates

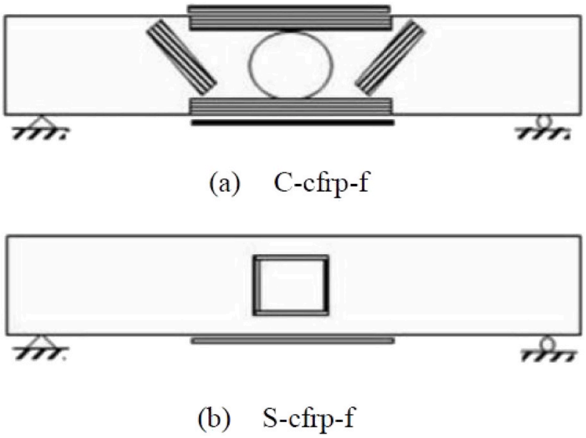

Fig. 4. Strengthening arrangement [27].

S-cfrp-f was strengthened using FRP to fortify the square opening. The flexural cracks formed outside of the area resisted by FRP during the beam test conducted. As the number of fractures increased, the crack propagations occurred at the beam's neutral axis, and another appeared diagonally near the support. The diagonal crack widened as it moved toward the load's origin and ultimately failed. The beam failed in a flexure mode, as seen in Fig. 6. The FRP developed cracks at the beam's base, and the concrete covering began to peel away from the FRP. Furthermore, the cracks in the applied load area penetrated the aperture corner on the top chord. This penetration resulted in a sudden concrete crushing due to the main longitudinal bar yielding located above the opening. As a result of the tension and compression stresses exerted on the beam by the applied load, the FRP on the opening's top and bottom inner surfaces were bent and delaminated from the opening's surface. When comparing the beams with different openings, it was common to find that circular opening was stronger than square opening. The stress might be so great in the four corners of the enormous square aperture when the cracking fracture began. The presence of diagonal FRP near the large circular opening appeared, causing an increase in the ultimate capacity of C-cfrp-f beam. The diagonal laminates interrupted the crack propagation's natural path direction, requiring higher energy potential to redirect the crack propagation direction through the unreinforced area without FRP. S-cfrp-f opening was square, and the flexural fractures could find the unreinforced area that the FRP did not control, resulting in a reduced capacity. By reducing the additional strength applied to "C-cfrp-f" and increasing the ultimate capacity applied to "S-cfrp-f," an efficient strengthening setup could be provided. Table 2 shows the experimental test results.

Fig. 5. C-cfrp-f [27].

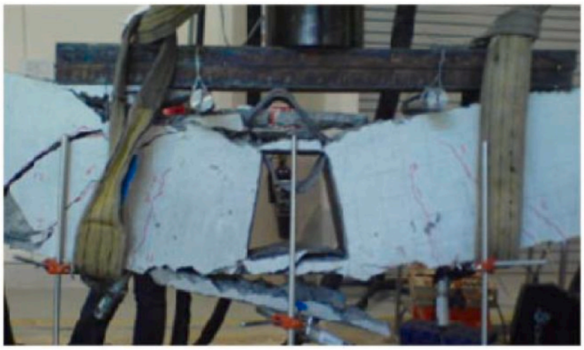

Fig. 6. S-cfrp-f [27].

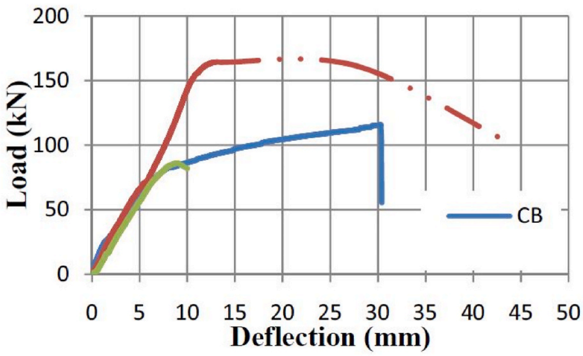

Fig. 7. Load-deflection of CB, C-cfrp-f, S-cfrp-f [27].

Table 2
Experimental test results [27].

Beam	Pu (kN)	Mode of Failure
CB (Control)	115.67	Shear
C-cfrp-f	164.40	Shear at opening
S-cfrp-f	86.07	Flexure at opening

3.2. (Siew Choo Chin et al., 2015) [28]

The beam samples used in this research are summarised in Table 3. All beams were tested after curing for a week after applying the CFRP on the beams' lower surface.

The shear region between the loading point and the support developed diagonal cracks, ultimately leading to the failure of both control beam (CB) and unstrengthened beam with openings (NS–BCO). The cracks for CB propagated vertically from the beam's edge along the flexural zone, as seen in Fig. 8(a). The failure occurred in shear, as seen in the NS-BCO in Fig. 8(b). For CB, the flexural cracks occurred along the tension zone. It was observed that two separate diagonal cracks were propagated, starting from the loading to the opening and the opening to the support upon the beam failure. SS-BCO was strengthened with no flexural cracks found along its mid-span, as observed in Fig. 8(c). The surface strengthening showed no indications of FRP debonding. There were some minor diagonal cracks on the CFRP surface in the shear span on the holes' top and bottom chords. Additionally, the other surface of the SS-BCO beam without CFRP external reinforcement showed diagonal fissures, ultimately leading to the beam's failure under increasing loads. Fig. 9 compares the load-deflection curves of a deep beam with a circular opening to a non-strengthened deep beam and a CB. The greatest

Table 3
Beam specimens [28].

Beam	CB	NS-BCO	SS-BCO
Centre distance from support (mm)	–	135	135
Shape	–	Circular	Circular
CFRP wrap	–	No	Yes

a) Control Beam

b) RC Deep Beam with Circular Openings (NS-BCO)

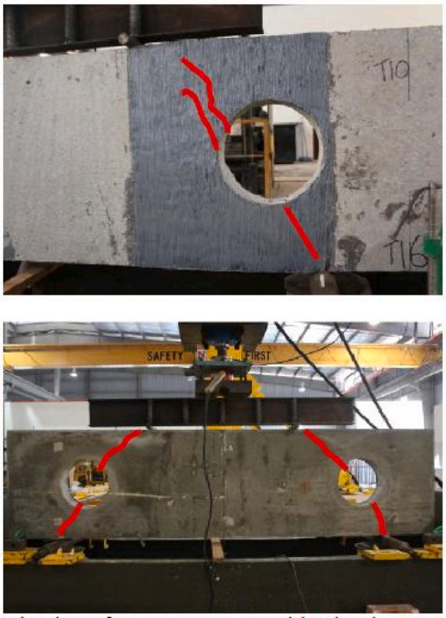

c) Surface Strengthening of RC Deep Beam with Circular Openings (SS-BCO)

Fig. 8. Failure mode, crack pattern [28].

load the beam could support, as determined experimentally for CB, was 425.12 kN, with a resulting deflection of 12.79 mm. The NS-maximum BCO's beam load was 207.47 kN at 8 mm deflection, which resulted in 51% declination compared to CB due to large circular gaps in both shear spans. The strengthened beam, SS-BCO, could carry 239.29 kN load, 10.9 mm deflection, referring to the load-deflection curve. The CB's structural capacity was only 56% restored with the surface strengthening configuration. The results show that the beam capacity, deflection behaviour, and ductility before failure were all improved by using a surface strengthening

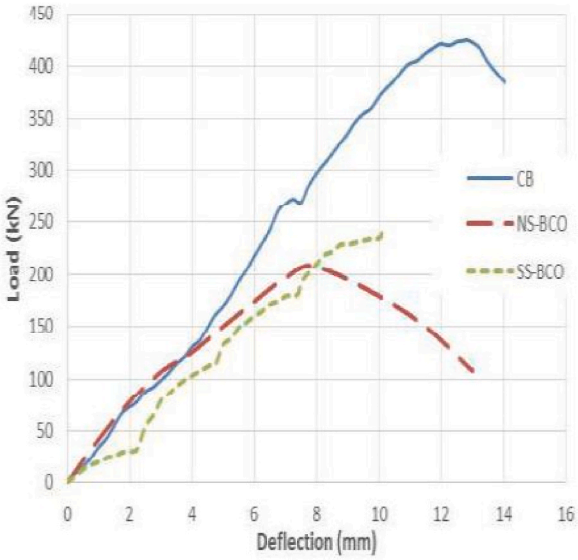

Fig. 9. Load-deflection [28].

technique involving CFRP's vertical alignment around the circular opening. Table 4 provides the findings summary from the experimental tests conducted. The analysis of fracture patterns revealed that the crack pattern occurred in the unstrengthened beam with large circular openings on the right shear span, indicating a failure of frame type. There were two separate diagonal cracks occurred, one in each chord member located above and below the aperture. However, the crack pattern seen in the reinforced beam with the round perforations indicated a failure. The failure plane was tilted at an angle of 45°, as in Fig. 10(a) and Fig. 10(b). The beam failed analogously to the solid beam, with the plane passing through the hole's exact centre. This indicated that frame-type failure occurred in the unstrengthened beam and converted to beam-type failure because of the CFRP strengthening on the beam surface area with a large circular opening Table 5.

3.3. *(Laminates et al., 2014) [29]*

System V was used to reinforce the beams. The strengthening System V, which included FRP plates and epoxy, is delineated in Fig. 11. Beam CP1–V had two 80-mm broad plates attached to its underside across its width. Similar to Beam CP1–V, Beam CP2–V was reinforced by adding plates to both ends for one-fourth of the beam's cross-depth section. Both ends of the beam were covered with a single plate 80 mm (3.1 inches) broad. Beam CP3–V underwent the same strengthening process as Beam CP2–V by adding a 50 mm (2.0 inches) wide plate on each side and an 80 mm (3.1 inches) plate. The plates were stuck along and parallel to the beam span.

CFRP had a special property which improved and increased the external reinforcement strength. The load-deflection for all beams is depicted in Fig. 12. A 66.7 kN load resulted in 22 mm, 14 mm, and 25 mm deflections, respectively. Above the breaking stress, where the FRP plates were the most effective in enhancing the beams' stiffness and caused differences in deflections. Compared to steel, the FRP plate improved the reinforcing ratio of the beam due to its high modulus of elasticity. Beam CP3–V, reinforced with FRP plates on the bottom and half of its sides, had the lowest deflection at its ultimate load and carried the highest weight. Based on the findings in Fig. 13, the presence of FRP plates apparently altered the compressive strain pattern in the concrete. The steel bars in the unreinforced beam were subjected to increase stress until they reached their yield strength. After that point, the concrete's compressive strain was less increased because the steel was deformed to absorb most of the added stress. This is because the strengthened beams' tensile stresses were distributed over the steel bars and the strengthening plates. The steel bars' stress was reduced and might even be lower than the material's yield strength. Thus, the strengthened beams experienced greater concrete strains than the control beam under the same load. Fig. 14, Fig. 15, and Fig. 16 delineate the failure mode of all beams, respectively. Connecting FRP plates to the beam sidewalls reduced the crack propagations. Moreover, including FRP plates on the beam's sides did not alter the crack's inclination angle since they only carried stress in their longitudinal direction and did not carry any shear force. The tension caused all beams to

Table 4
Test results [28].

Specimen	CB	NS-BCO	SS-BCO
Pu (kN)	425.12	207.47	239.26
Deflection (mm)	12.79	8	10.9
Strength regain (%)	–	–	56
Reduction (%)	–	51	–

Table 5
Tested beam details [29].

Beam	FRP strengthening
CP1–V	Bottom
CP2–V	Bottom & ¼ sides
CP3–V	Bottom & ½ sides

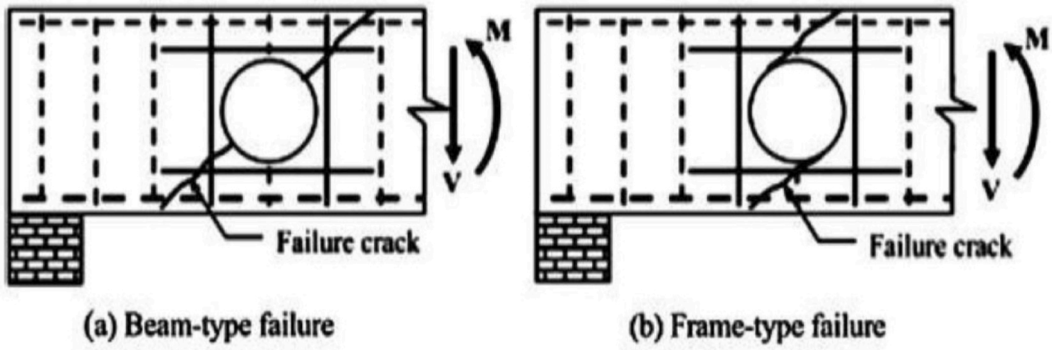

Fig. 10. Shear failure [28].

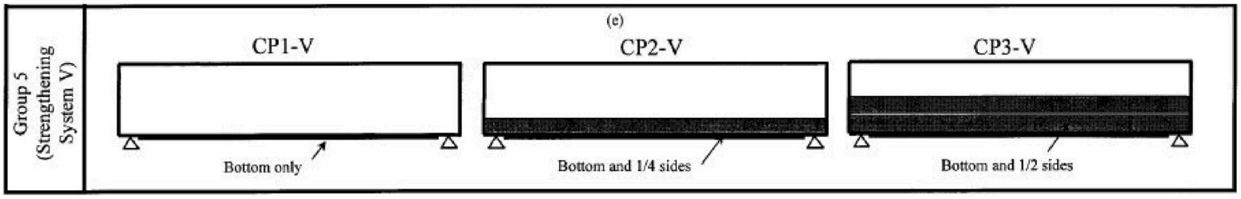

Fig. 11. FRP's strengthening arrangements [29].

break down, and the concrete near the FRP plates horizontally failed in shear. The three tested beams showed no signs of delamination or fibre breakage. As a result, when combined with FRP plates, it was proven that a more durable beam was produced than a normal reinforced concrete beam without FRP. Furthermore, the stress concentration was also increased with FRP plate usage, causing concrete shear failure to occur.

3.4. (Pham & Hao, 2016) [30]

Some RC beams have been effectively strengthened with longitudinal FRP to improve the compressive and flexural resistance in quasi-static tests. Various longitudinal FRP strips were used by attaching to the beam's lower surface area. However, the debonding of the longitudinal FRP strips reduced the efficiency of this strengthening method. There are a variety of factors that could cause longitudinal FRP strips to become unattached. Typically, debonding failures occurred at or near the FRP plates attached. High interfacial shear and normal stress caused this failure. Furthermore, debonding became essential as FRPRCB was subjected to impact loading. The beams strengthened with FRP were debonded against impact loading and causing the beam strength to increase gradually. A phenomenon comparable to the static aspect was discovered in an analytical investigation of RC beams strengthened by FRP under impulsive loads created by peeling stress at the FRP's origin. Impact loading was a state of exceptional severity in which a large force was applied rapidly and with tremendous intensity. Two distinct phases of response might characterise the behaviour of structures when subjected to impact loading. The elastic-plastic deformation influenced the force and vibration after the long persistent impact. The stress wave immediately produced the local response at the loading point because the impact occurred in a short time. It was important to remember that the loading range and rate affected the dynamic behaviour of the structural element members and controlled the overall reaction to a large extent. There might also be significant differences between FRP and concrete attachment observed in static and impact tests. Due to the combined effects, the bond strength of FRP might suffer if the material was subjected to stress during these two phases.

3.5. (Karayannis et al., 2018) [31]

An experiment with four-point loading was performed on five beams. The five beams used FRP bars as tensile reinforcement. There

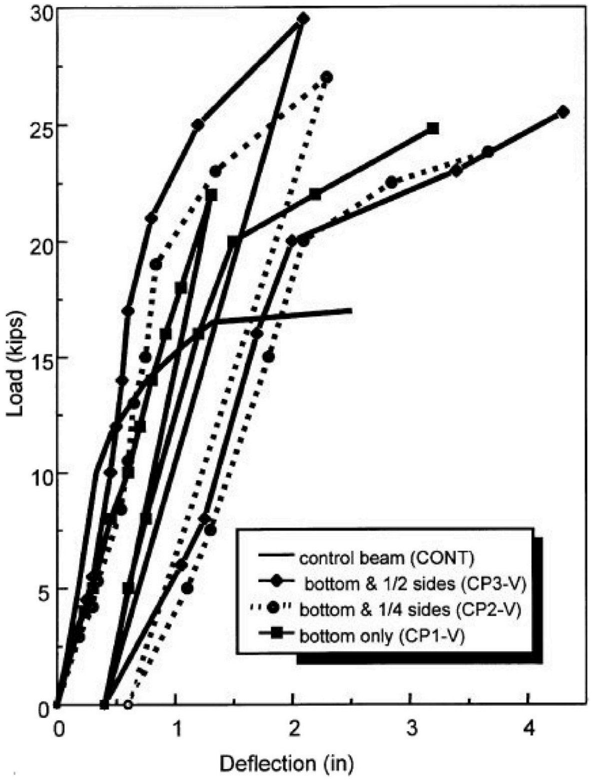

Fig. 12. Load-Deflection [29].

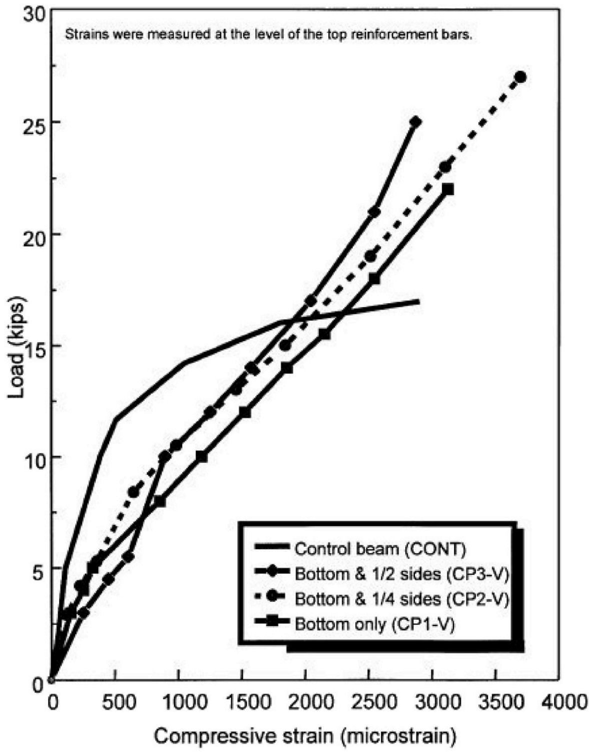

Fig. 13. Load-Compressive strain [29].

Fig. 14. CP1-Vand 8(k), (l), and (m) [29].

Fig. 15. CP2–V [29].

Fig. 16. CP3–V [29].

were two categories ("BF5" and "BF10") for RC beams made using FRP bars. In group BF5, the specimens were labelled as BF5-0, BF5-1 and BF5-2. For group BF10, the specimens were labelled as BF10-0 and BF10-1. The specimen details are shown in Table 6.

The load suddenly dropped when the fracture developed on the surface of the FRPRCB as shown in Fig. 17(1), Fig. 17(2), Fig. 18(1), Fig. 18(2), Fig. 19(1), Fig. 19(2), Fig. 20(1), Fig. 20(2), Fig. 21(1), and Fig. 21(2). The combination of long flexural cracks and low elastic modulus of FRP bars caused this fracture. A local stiffness loss occurred at the beam's cracked part. Before cracking, the member's stiffness was high because the entire concrete cross-section was used. After cracking, only the concrete compressed part was effective. In contrast, the FRP tensile bars' contribution was relatively smaller because of the material's low modulus of elasticity. As a result, when the beam's cross-section was uncracked, a lower applied loading was needed to create the same deflection as the fractured

Table 6
Experimental results [31].

Beam	Type and diameter
BF5-0	2HD5.5
BF5-1	2HD5.5
BF5-2	2HD5.5
BF10-0	2HD10
BF10-1	2HD10

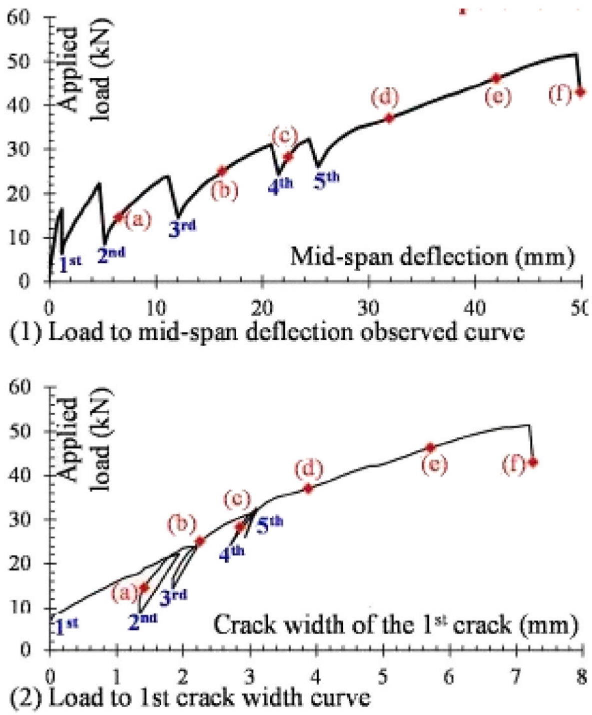

Fig. 17. BF5-0 [31].

occurred. A beam with a minimal value of the normalised reinforcement ratio f (Ef/Ec) was particularly susceptible to this effect. The enhanced anchoring conditions for FRP bars improved the bond behaviour between the bars and the concrete, enhancing the flexural behaviour. Due to the significantly greater modulus of elasticity of the steel bars compared to one of the FRP bars and the relatively high s (Es/Ec), the decreasing load was not observed for steel RC beams. Due to low axial stiffness, the cracking occurred more rapidly in the early stages of FRPRCB than in steel-reinforced beams. The cracks were also propagated slower, and no loading drops were observed when the crack appeared. From the identical vantage point, it could be seen that the beams from "BF10" group, reinforced with FRP bars with a larger diameter, produced greater stiffness and experienced a smaller loading decrease than "BF5" group. It should also be emphasised that BF5-1 and BF10-1 beams with local spiral confinement reinforcement did not exhibit smaller and weaker loading decreases. The FRP bar's poor axial stiffness might cause this case. Calculating axial stiffness was as simple as multiplying the cross-sectional area (A_s) by the modulus of elasticity (E_f). Due to low A_fE_f, every new crack immediately grew up vertically to the compression zone. At the same time, the initial split was clearly widening. The placements of the vertical stirrups were emphasised as the origins of all cracks that had occurred.

3.6. (Narayanan, 2021) [32]

Five reinforced concrete beams were investigated with different properties. One was unplated without FRP (control), and the other four were 3.5 mm thick plating of CSM, WR, UD, and CSMWR. The CSM, WR, UD, and CSMWR were the types of FRP-wrapped methods on the beam's lower surface. Table 7 summarises the specimen details.

The load-deflection curves for five different beams are depicted in Fig. 22. The GFRP-plated beams carried more weight and could support a greater load at a given level of distortion than the unplated beams. The load-deflection data are summarised in Table 8. The first fracture loads of SRWR were 71.43% higher than the control specimen (SR). Compared to SRCSM, SRWR produced a greater increase in yield load. The deflection was reduced when CSM laminates were used instead of WR during plating. Given that CSM

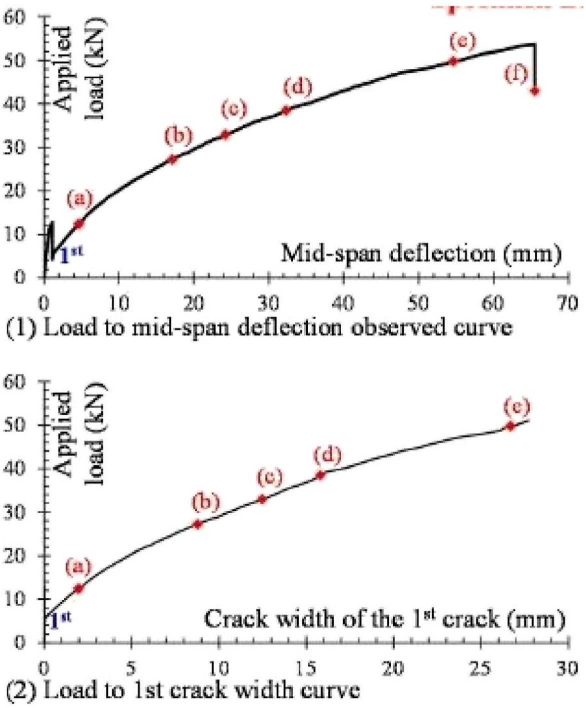

Fig. 18. BF5-1 [17].

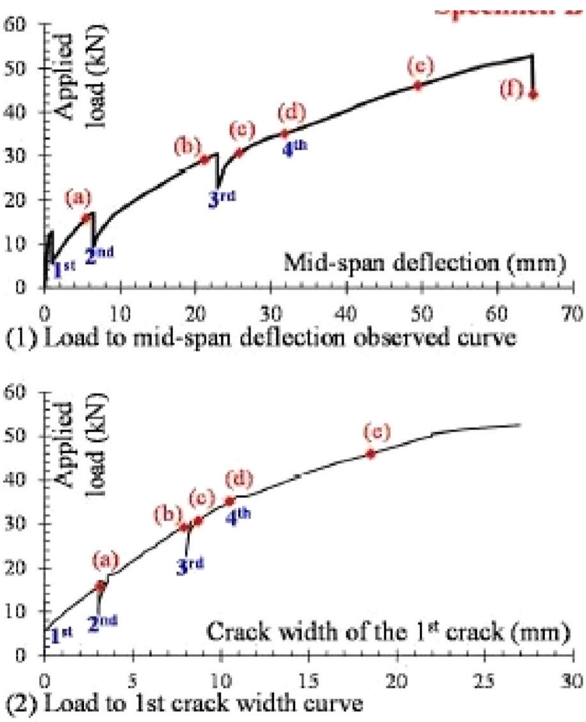

Fig. 19. BF5-2 [31].

achieved a lower yield load than WR. This might not be interpreted as a signal of improvement in stiffness value. Ultimate strength values were achieved via WR fibre-reinforced laminate and were greater than those achieved using CSM-reinforced laminates. Tabular data for energy ductility and deflection are provided in Table 9. Beams plated with GFRP revealed a decrease or barely noticeable rose

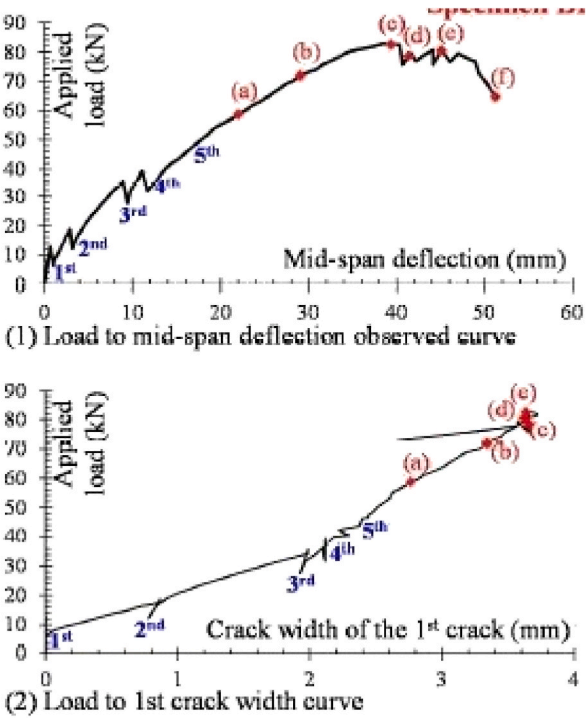

Fig. 20. BF10-0 [31].

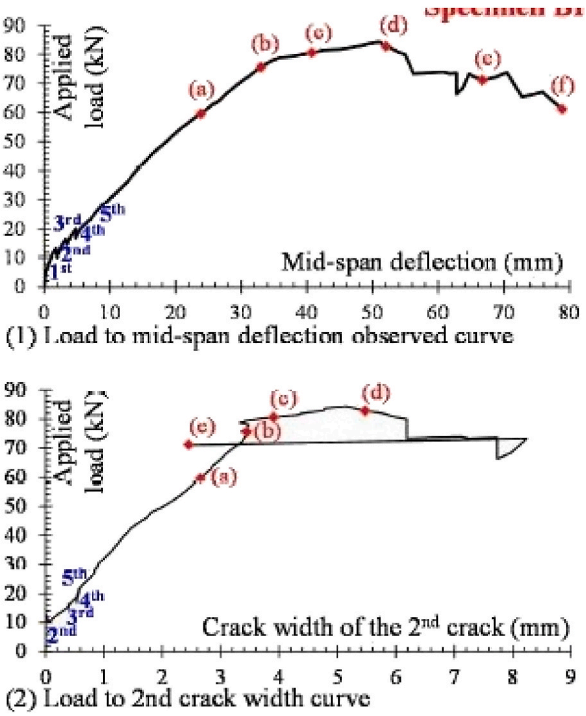

Fig. 21. BF10-1 [31].

in deflection ductility values. The deflection ductilities of SRCSM, SRWR, SRUD, and SRCSMWR beams were increased by 50.57%, 56.29%, 5.18%, and 64.48%, respectively, compared to SR. Beams with greater GFRP thickness exhibited greater energy ductility. The energy ductilities were improved by 74.01%, 117.32%, 29.40%, and 118.90% for SRCSM, SRWR, SRUD, and SRCSMWR compared to

Table 7
Specimen details [32].

Beam name	GFRP type
SR	–
SRCSM	CSM
SRWR	WR
SRUD	UD
SRCSMWR	CSM + WR

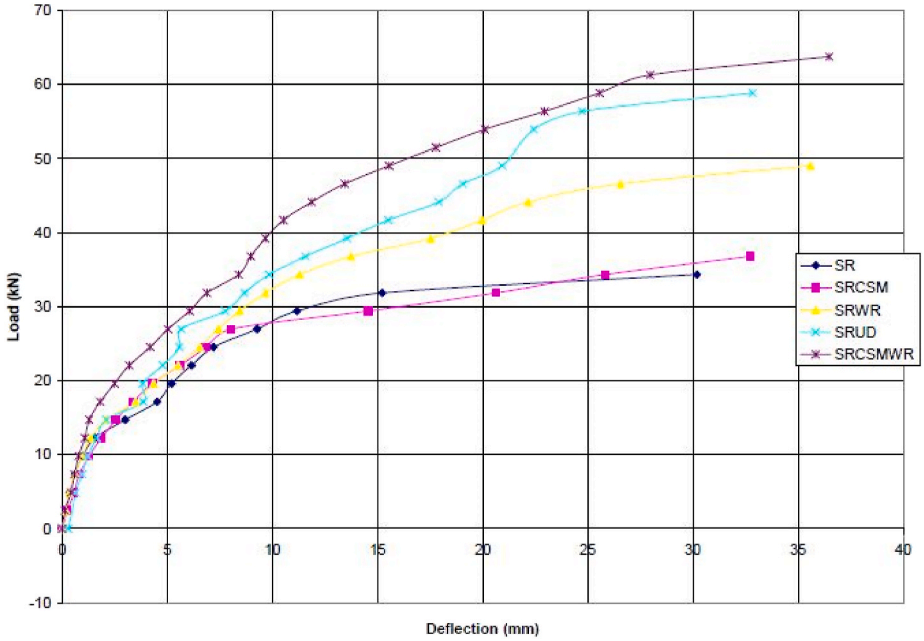

Fig. 22. Load-Deflection [32].

Table 8
Test value results [32].

Result/Beam	SR	SRCSM	SRWR	SRUD	SRCSMWR
1st crack load (kN)/deflection (mm)	17.17/4.52	17.17/3.38	24.53/6.55	29.43/7.77	34.34/7.39
Ultimate load (kN)/deflection (mm)	34.34/30.20	36.79/32.73	49.05/35.60	58.86/32.83	63.77/35.49
Yield load (kN)/deflection (mm)	17.17/11.17	22.07/8.04	39.24/8.44	44.15/11.58	5.50/7.98
Maximum crack width (mm)	1.20	1.00	0.60	0.82	0.62

Table 9
Energy and deflection [32].

Result/Beam	SR	SRCSM	SRWR	SRUD	SRCSMWR
Energy ductility/ratio	3.81/1.00	6.63/1.74	8.28/2.17	4.93/1.29	8.34/2.11
Deflection ductility/ratio	2.70/1.00	4.07/1.51	4.22/1.56	2.84/1.05	4.45/1.64

SR. Applying GFRP plating on the beam surface helped to boost the strength and ductility simultaneously. The energy ductility was shown to be significantly affected by the thickness of the GFRP plating, with a greater increase for a greater plating thickness.

3.7. (Venkatesha et al., 2013) [33]

Table 10 shows the details of the beam specimens used. All beams with 25 mm concrete cover with three different stirrup spacings (100 mm, 120 mm, and 125 mm). The beams' dimension was 100 mm × 200 mm x 1500 mm and were reinforced with 2 bars of 12 mm diameter for the main reinforcements, 2 bars of 6 mm diameter for the hangers, and 2 bars of 6 mm diameter for the stirrups. WSB1,

Table 10
6 specimen details [33].

Beam	CFRP	Stirrup details
SB1	No	6H-100
WSB1	U-Wrap	6H-100
SB2	No	6H-120
WSB2	U-Wrap	6H-120
SB3	No	6H-125
WSB3	U-Wrap	6H-125

WSB2 and WSB3 beams were wrapped with FRP. Table 11 displays the ultimate and initial crack loads. Based on the data obtained, both ultimate and initial crack loads increased for WSB1, WSB2, and WSB3 compared to control beams (SB1, SB2, SB3) without FRP. The increasing percentages were 5.11%, 16.42 and 18.11% for WSB1, WSB2, and WSB3. The failure mode shifted for the second and third control beams, where (a/d) were 1.85 and 1.71, respectively. Whether or not the wraps were presently affected, the prominent crack that eventually led to failure was formed. Failure in SB2 and SB3 beams happened as the major fracture propagated from the shear zone, while failure in the FRP-wrapped beams (WSB2 and WSB3) occurred as the cracks propagated vertically in the flexure zone, albeit more or less under one of the loading points. The FRP-wrapped beams experienced explosive failure because the wrap and the thin layer of concrete parted at the compression zone in one or both areas. Indeed, lateral bending was also seen in WSB1 beam when the FRP wrap was removed. These findings, with a lack of discernible, increased the beams' ultimate strengths. The FRP wrap in the shear zone should have been continuously developed. The orientation of the FRP fibres in the flexure zone was parallel to the neutral plane of the beam. It should be emphasised that the FRP wrapping method adopted in this investigation shifted the beam's failure mode from shear to flexure. In conclusion, the FRP affected the beam's load values and failure modes (Fig. 23) by increasing its structural behaviour. FRP contained fibre properties which affected the beam's structural performance. The fibre caused the beam to become stronger compared to the control beam without FRP wrapping.

3.7.1. (Rahman et al., 2005) [34]

Table 12 depicts the beam specimen details. The reinforced concrete beam dimension measured was 150 × 255 × 2400 mm (w × d × h). B2GL and B3GM beams were reinforced with FRP bars of 3@16 mm diameter, whereas the control beam B1SSL was strengthened with deformed austenitic stainless steel bars. Both B1SSL and B2GL beams had simple stainless steel bars with a diameter of 6 mm used to strengthen them against shear force. Beam B3GM's shear reinforcement used 304 stainless steel mesh with a 3 mm diameter and 50 mm square opening. Flexure failure was intentional for all of the tested beams.

Fig. 24 depicts the load-deflection behaviour of 3 tested beams. All beams exhibited linear elastic behaviour up until the load increased at the tension area. The beams' rigidity dropped more rapidly, especially for the FRPRCB, causing more bending to occur. The FRP bars had a lower elastic modulus compared to the stainless steel bar. The deflection of beam B2GL was approximately 2.5–3.0 times bigger compared to the control beam (B1SSL). A near-failure deflection of 21.7 mm was reported for B1SSL, and a deflection of 35.1 mm was measured for B2GL. The performance of a beam reinforced with FRP bars will be inferior to the steel-reinforced beam even if the beam was replaced with FRP bars at the same area replacement. Therefore, various design modifications must be addressed when FRP bars are utilised as reinforcement. The B3GM's rigidity was slightly enhanced due to the addition of stainless steel mesh shear reinforcement. That stainless steel mesh with FRP was used as shear reinforcement not only increased the stiffness of the beam but also enhanced the reinforcement to resist shear load. At the same load point, the deflection ratios of B3GM and B1SSL were 2.0–2.7, representing a smaller increase compared to the identical beam equipped with links as shear reinforcement. When the beam was almost at its failure point, the deflection measured was 34.5 mm.

After the flexural cracks developed, all the tested beams failed in flexure, and the concrete was crushed in the compression zone at the failure stage. The failure mode and crack pattern of the tested beams are presented in Fig. 25. Table 13 shows the crack details. All beams broke in tension at a load between 8% and 11% of their ultimate capacity. In the area of maximum bending moment, the first crack appeared between the two-point load locations. As the load increased, more cracks started to form over the shear span on both beam sides. The cracks were about 25% lower, and the crack spacing was about 26.6% larger for B2GL compared to the control beam (B1SSL). This might indicate that the FRP bar's stiffness affected the beam's cracking behaviour. In contrast to B1SSL and B2GL, B3GM with stainless steel mesh as shear reinforcement experienced greater cracks with smaller crack spacing. B3GM had a 28% smaller average crack spacing than B1SSL. This demonstrated that stainless steel mesh could lessen the cracking occurred for FRPRCB.

Table 11
Ultimate load and failure mode [33].

Beam	Ultimate load (kN)	Failure mode
SB1	100.92	Flexural
WSB1	106.08	Compression
SB2	134.92	Shear compression
WSB2	157.08	Compression
SB3	149.08	Diagonal shear
WSB3	176.08	Compression

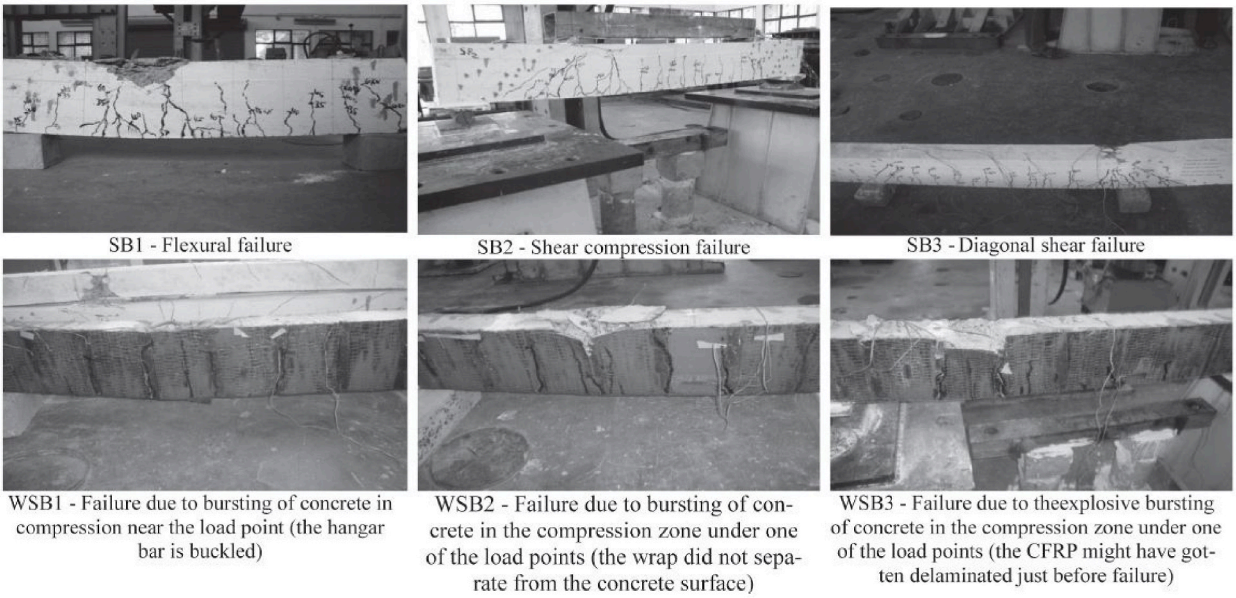

Fig. 23. Failure mode of all 6 beams [33].

Table 12
Details of specimen [34].

Specimen	Type of bar	Shear reinforcement
B1SSL	Austenitic stainless steel	Stainless steel bar (6 mm)
B2GL	FRP (3@16 mm)	Stainless steel bar (6 mm)
B3GM	FRP (3@16 mm)	Stainless steel mesh (3 mm diameter, 50 mm square opening)

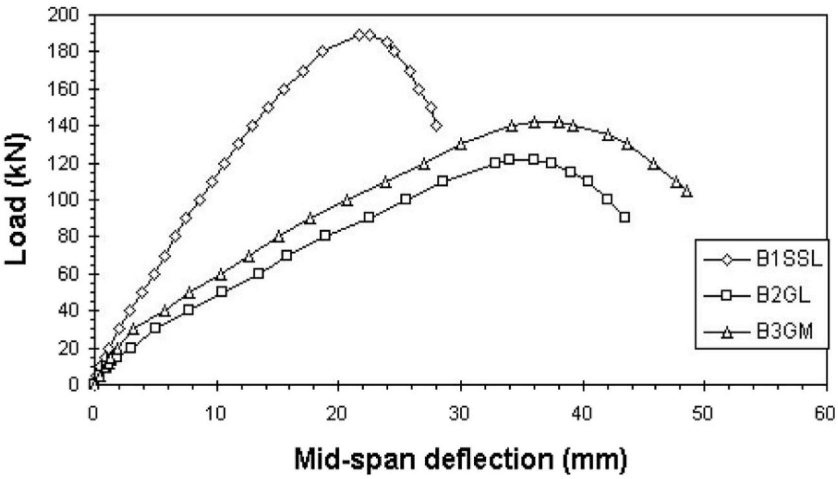

Fig. 24. Load-Mid span defelction [34].

3.8. *(Murugan & Kumaran, 2019) [35]*

Five beams were cast. The reinforcement ratios of 0.73% and 1.24% were used to cast two beams with sand-coated GFRP bars and two beams with grooved GFRP bars, respectively. 0.73% reinforcement ratio was used to investigate the differences between GFRP rods and conventional steel rods. The steel rods were attached to the stirrups with mild steel wires, while the GFRP rods were bonded with stirrups using nylon zip ties. Table 14 shows the various beam designations.

The ultimate loads of sand-coated (Bm1sp1) and grooved rod-reinforced (Bm1Fegp1) beams were 34 KN and 38 KN, which were

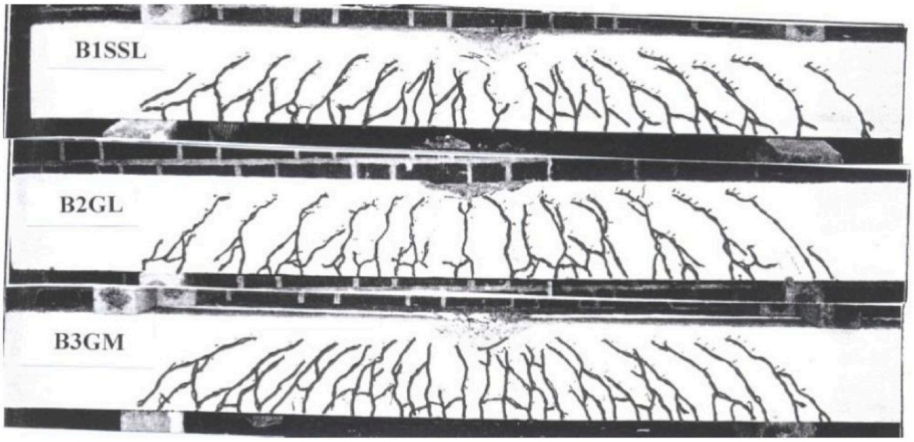

Fig. 25. Failure mode and crack pattern [34].

Table 13
Crack details [34].

Beam	Ultimate/1st crack loads	Cracks number/spacing
B1SSL	189/15	20/79
B2GL	122/13	15/100
B3GM	142/12	24/57

Table 14
Beam designations [35].

Beam	GFRP type	Ratio of reinforcement
$Bm_1F_eP_1$	Steel	0.73
$Bm_1F_sP_1$	Sand coated	0.73
$Bm_1F_sP_2$	Sand coated	1.08
$Bm_1F_gP_1$	Threaded	0.73
$Bm_1F_gP_2$	Threaded	1.08

15% and 5% lower compared to the steel-reinforced beam (Bm1Fep1). When the reinforcement ratio of GFRP beams rose to 1.08%, the ultimate load rose to 50 kN and 56 kN, representing increased of 25% and 40% more than the sand-coated and grooved rod-reinforced beams, respectively. Increasing the reinforcing ratio in GFRP-reinforced beams raised the beam's ultimate load. An increase in the reinforcing ratio resulted in a smaller ultimate deflection for grooved rod beams compared to sand-coated rod beams. The moment-curvature behaviour of all five beams was monitored during the static loading phase. Fig. 26, Fig. 27, and Fig. 28 depict the load-deflection, moment-curvature and stress-strain of all five beams. The higher the concrete and steel material properties, the higher the moment-curvature relation. This is because high steel properties contained a high tensile load which influenced the section's

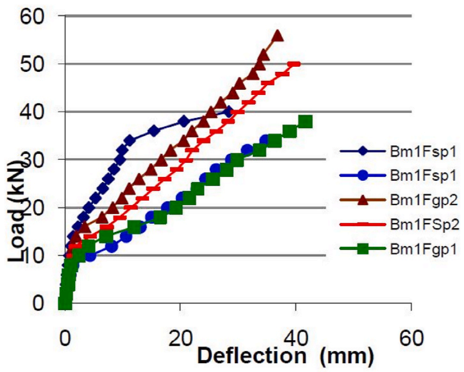

Fig. 26. Load-deflection [35].

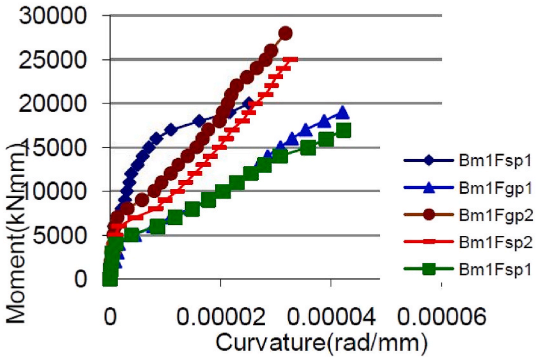

Fig. 27. Moment-curvature [35].

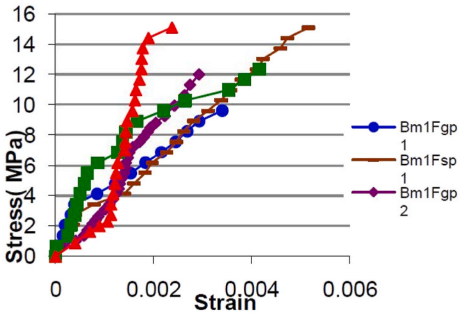

Fig. 28. Stress-strain [35].

moment-curvature relation. In addition to this, the elastic bending stiffness (EI) was also equal to the gradient of the moment-curvature relation under normal loading. Table 15 shows the data results of all five beams.

3.9. (Yang, 2021) [36]

As seen in Table 16, the control specimen (TB1) was not reinforced with CFRP plates. The remaining three specimens were reinforced with self-anchored prestressed CFRP plates, and the beam flange top was reinforced with prefabricated GFRP panels. The bond layer between GFRP panel and T-beam, and the configuration and prestressing percentage of GFRP panel were distinguished between TB2 and TB4.

The cracking loads increased from 19 kN for the control specimen (TB1) to 61–75 kN for specimens (TB2-TB4). The bending stiffness increased from 82% to 98% after the cracking stage compared to TB1 because of the tensile and compressive reinforcement between the RC cross-section, bonded CFRP plate, and GFRP panel. The abrupt load decreases for TB2-TB4 due to CFRP plate debonding after the steel reinforcement yielding, as delineated in Fig. 29. The tensile strains at the plates' midspan during debonding ranged from 10.4 to 10.9, equating to a utilisation ratio of 82–86% of the CFRP's tensile capacity. This ratio value was similar to the anchored prestressed CFRP plate. The hybrid FRP strengthening system enhanced the beams' cracking control, bending stiffness and load-carrying capacity. Significant residual capacities were observed in the reinforced specimens after debonding period (referred to as post-debonding phase). It successfully achieved and maintained high residual capacities due to the GFRP panel mounted. It served as compressive reinforcement and absorbed most of the compressive force applied to the bending specimens after they were strengthened. The concrete was crushed at T-beam tops even though the load increased from 350 kN to 400 kN (2.3–2.6 times the maximum load of TB1) because the compressive zone was shifted to GFRP panel during post-debonding phase. The inclination of the external load is depicted in Fig. 30, which depicts the growth of maximum crack widths. The crack-width growth curve magnitude and gradient

Table 15
Experimental results [35].

Beam	Crack width (mm)	Ultimate load (kN)-Deflection (mm)
$Bm_1F_eP_1$	0.52	40–28.40
$Bm_1F_sP_1$	0.78	34–34.80
$Bm_1F_sP_2$	0.82	50–39.62
$Bm_1F_gP_1$	0.84	38–41.68
$Bm_1F_gP_2$	0.90	56–36.85

Table 16
Specimen details [36].

Beam	Bond layer thickness
TB1	No
TB2	10 mm epoxy
TB3	30 mm mortar
TB4	30 mm mortar

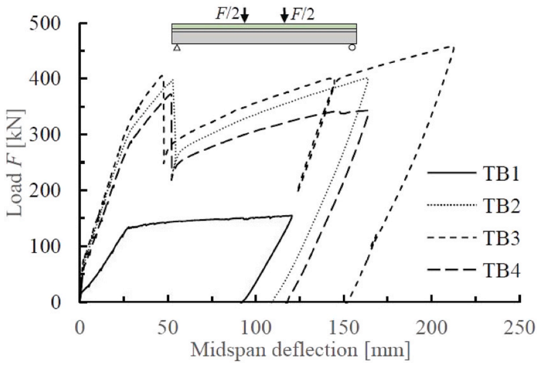

Fig. 29. Load-Mid span deflection [36].

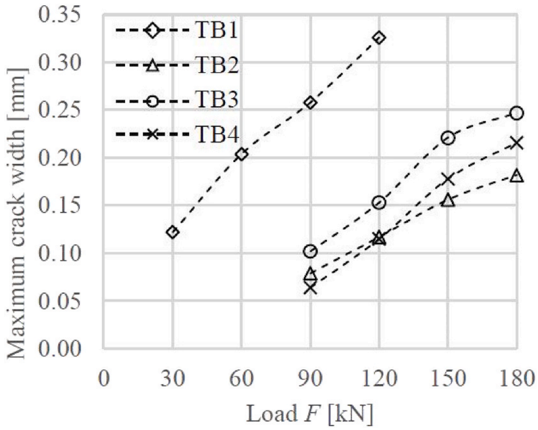

Fig. 30. Max crack width-Load [36].

were reduced for strengthened specimens (TB2-TB4) compared to the control specimen (TB1).

3.10. (Ahmed et al., 2021) [37]

The effects of strain rates and temperatures on CFRP composites were being studied. The strain rates and temperatures also affected the CFRP composites. Strain rates between 4 $\times$ 10^{-5} and 160 s^{-1} were recorded for UD and plain CFRP laminates, while similar findings were reported for UD CFRP composites at strain rates of 25, 50, 100, and 200 s^{-1} and temperatures of 25, 0, 25, 50, 75, and 100 °C. The effects of layup (stacking sequence of the laminates), strain rate, and high temperature on the mechanical behaviour of CFRP composites were studied using quasi-static and dynamic experiments. It was discovered that the CFRP composites had strain rate strengthening effects, but a high temperature will weaken the strain rate. Temperature also played a significant role in determining the tensile performance of short carbon fibre-reinforced poly-ether-ether-ketone composites. As the temperature rose, both tensile strength and modulus dropped, but the fracture strain rose. The strain rate affected CFRP composites' tensile, compressive, and shear characteristics. The composites' stiffness and strengths (compressive, tensile, and shear) significantly rose as the strain rate was increased to roughly 200 s^{-1}. When tested at strain rates of 1.5–2.5 mm/min at temperatures of 35–70 °C, CFRP composites were found to have superior tensile and flexural characteristics over GFRP composites. The damage initiation locations were found due to temperature and strain rate dependence. The failure modes of CFRP specimens were temperature dependent rather than strain rate dependent due to the polymer matrix's softening at the glass transition temperature. The stiffness was reduced due to the loading and softening impact on the interfaces between fibres and matrices. Since the characteristics of CFRP composites were sensitive to temperature and strain change, designing for structural elements with severe temperatures and dynamic loadings was essential. In general, the FRP (CFRP and GFRP)'s tensile characteristics, and failure mechanisms were susceptible to the strain rate and temperature at which they were being applied to the beam specimens.

3.10.1. (Naser et al., 2019) [38]

Attaching FRP plates, strips, or fabrics at the soffit of simply supported beams with an external bond increased the flexural capacity. Several failure modes were found when RC beams and slabs were experimentally strengthened with FRP laminates. Common failure

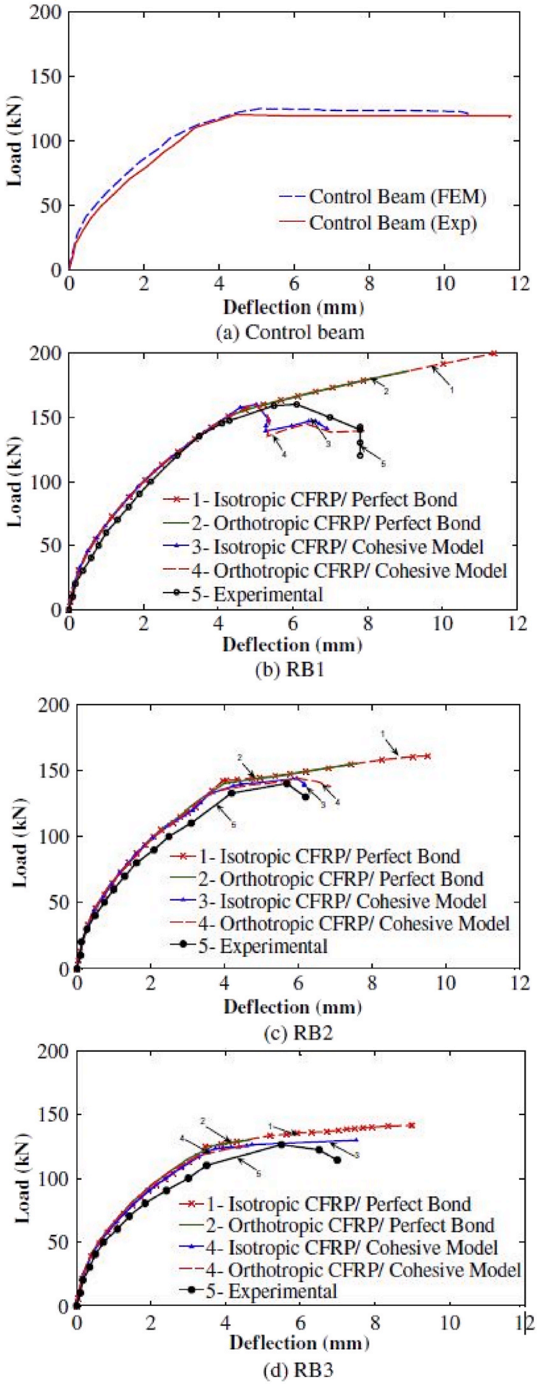

Fig. 31. Load-Deflection [40].

modes of strengthened RC members in flexure with FRP laminates included steel yielding followed by rupture of FRP laminates, FRP debonding from adjacent concrete surface, and concrete cover separation. If the FRP achieved its ultimate strain before the fibre concrete in the top compression reached its crushing strain, the externally bonded FRP laminate would be ruptured. If the concrete substrate could not withstand the axial force in the flexural FRP reinforcement, then FRP debonding or cover delamination would occur. Debonding of FRP laminates often began with flexural and/or flexural-shear cracks around the maximum moment area of the reinforced member and then propagated throughout the FRP length, including the bonding agent (epoxy adhesive or cement matrix). As these cracks propagated and spread under load, the shear stress built up at the FRP interface sheets/plates and the concrete substrate eventually led to FRP debonding. Debonding brittle failure modes included concrete cover delamination, which was typically triggered by the development of cracks at a high-stress concentration point close to the end of FRP laminate. Once the fracture reached the flexural steel reinforcement level, the concrete cover would begin to separate. When a crack developed in the concrete cover closed to the plate's terminus, this would cause the cover to fail. As the crack widened, it separated the RC beam's or slab's concrete surface from the rest, reaching the steel tension reinforcement level.

3.11. *(Muciaccia et al., 2022) [39]*

The bond strength of FRP anchors was significantly affected by the construction technique quality and the dryness or impregnation of the dowel component of the FRP anchor. First, the binding strength of FRP anchors might be drastically diminished due to improper hole preparation, improper adhesive placement, or nonvertical anchor, known as fibres misalignment. Next, it was advisable to round the hole corners at least 13 mm while installing bent anchors to reduce stress concentration. The borehole diameter unaffected the anchor's tensile strength, although a gap of 2 mm was advised for better placement of epoxy around the anchor. Because the FRP were less well aligned with the applied force direction, the efficiency of straight anchors fell dramatically as the insertion angle increased. Then, the anchor's strength depended on the CFRP's fibre ratios to form them to the attached fibres. Anchors from CFRP should have a cross-sectional area at least twice as large as the CFRP reinforcement sheet mounted. This problem had a significant impact on the retention and failure performance of the FRP sheet just before the FRP anchor failed. After that, to be functional, an FRP anchor should be at least 13 mm longer than the FRP's width, followed by 60° maximum angle. It was suggested that the anchors overlap by at least 10 mm by putting them next to one another. Finally, as a general rule, more anchors of smaller diameter were better than fewer anchors of bigger diameter.

4. Finite element analysis of fibre reinforced polymer reinforced concrete beams

A state-of-the-art review of finite element analysis (FEA) on the structural behaviour of fibre reinforced polymer reinforced concrete beams (FRPRCB) is discussed in this section.

4.1. *(Obaidat, 2022) [40]*

Fig. 31 displays the experimental and FEM analytical load-deflection curves for the control and retrofitted beams. Four different setups involved an FRP model and a concrete/FRP bonding model. For the control beam shown in Fig. 31(a), there was a good agreement between FEM and experimental results. The beam was expected to be slightly stiffer and stronger than the FEM study predicted, most likely due to the projected perfect bond between concrete and reinforcement. The high degree of concordance caused the fracture behaviour and could be captured effectively by the constitutive models which were typically used for concrete and reinforcement. From Fig. 31(a), (b), Fig. 31(c), and Fig. 31(d), it was clear that the FRP length significantly impacted the beam's behaviour. The maximum load increased with FRP length. Fig. 31(b)–(d) show that throughout the initial portion of the curve, all four FEM models for the retrofitted beams produced very similar results and were stiffer than experimental results. The beam lost its stiffness when fractures were formed and experienced an increase in shear strain. Once the cracks emerged, the perfect bond models consistently overestimated the beam's rigidity. This is because the perfect bond ignored the shear strain between the concrete and the FRP. The beam softening was especially noticeable for RB1, and the perfect bond models didn't capture it. The perfect bond model couldn't account for the debonding failure observed in the experiments. This means the load could be further increased until a different failure mode was reached. A shear flexural crack failure or FRP rupture had occurred. Isotropic and orthotropic perfect bond models produced nearly identical curves. However, the orthotropic model predicted a low maximum load. This might be because of the strengthening confinement of the isotropic FRP, which was unnaturally high stiffness in the transverse direction and shear. A good agreement between the cohesive models and the experiments was found. Both the isotropic and orthotropic cohesive models had very similar properties. The results revealed that, at least for large loads, the cohesive model agreed well with experiments, but the perfect bond model didn't. The discrepancies between the experiment and FEA could have several origins. One was the presumption of a complete bond between the concrete and the steel reinforcement for the control beam. It was also possible that the estimated behaviour of the interface between FRP and concrete was to blame for the discrepancy between the model and the experimental results regarding the pre-position cracks and dimensions. Because of this, the reinforced concrete element's stiffness and capacity might be overestimated. The findings also demonstrated that the orthotropic features of the unidirectional FRP could be disregarded.

A comparison of axial stress under a load of 10 kN between the control specimen and the modified beam (RB2) is depicted in Fig. 32 (a) and Fig. 32(b). This shows that the strengthening had systemic effects on the beam's stress distribution than the control beam without FRP. Besides that, the strengthened beams' stress distribution was far away differed from the unreinforced specimens' which didn't have FRP. This finding was confirmed across all models, including this FEA.

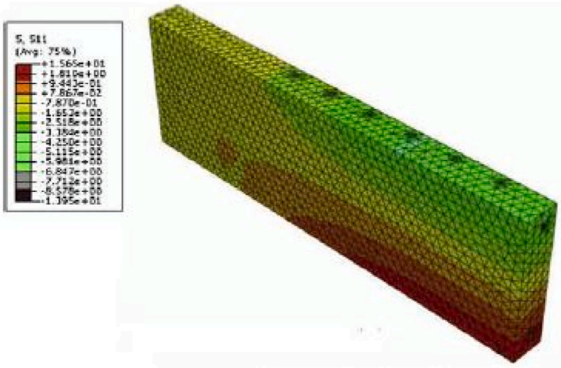

(a) Un-strengthened beam.

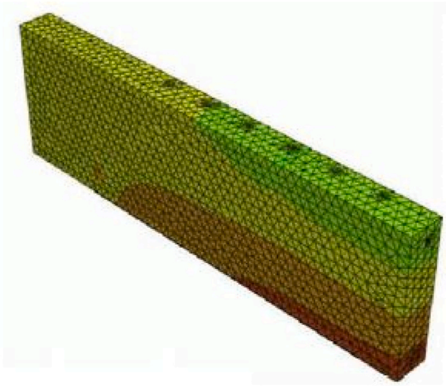

(b) Strengthened beam.

Fig. 32. Axial stress distribution (RB2) [40].

The crack propagation started at the locations where the maximal principal plastic strain was positive. It was anticipated that the crack propagation occurred at the material integration point. Fig. 33(a) and Fig. 33(b) show a contrast of plastic strain distributions and crack patterns for the control and strengthened beams with FRP between FEA and experimental investigation. This model could represent the beams' fracture mechanics demonstrated by the similarities between the cracks obtained from the experimental and simulation results. The perfect bond model could not model the debonding fracture mode seen in this study since it didn't seem eligible for bond breakage. However, the debonding could be modelled using a cohesive model. The debonding fracture occurred using a cohesive bond model as did in the experiment, as shown in Fig. 34 below.

4.2. (Bedon & Louter, 2019) [41]

For every kind of FRP reinforcement, two separate experiments were conducted. The obtained load-cross-head displacement relations for various FRP rebars are displayed in Fig. 35, Fig. 36, and Fig. 37. The initial findings emphasised the significance of the reinforcement area and section on the flexural behaviour of RCB. The failure loads of the samples were raised dramatically from 4921 N to 6121 N when 'dog-bone' sections were used for reinforcement rather than circular reinforcement. Both setups had comparable stiffness before the initial crack propagated. However, if the rebars had circular cross-sections at relatively light loads, the cracking and the resulting loss of stiffness began to appear. The dog-bone rebars maintained a fairly consistent stiffness from light loads until final failure. The moment of inertia of the dog-bone rebars was bigger than the circular rebars, which might explain this result by reducing stress, cracking and stiffness in concrete. In addition to that, the failure displacement was determined for the two arrangements and was very different from each other. Fig. 37 demonstrates that circular rebars resulted in a greater displacement to failure compared to dog-bone rebars.

The created finite element model (FEM) simulated the experimental results. There was a large amount of heterogeneity in the experimental results when the generalised cracking occurred in the specimens for displacement higher than 3.5 mm. The first non-linearity in the load-displacement relation, representing the onset of cracking, and the maximum load reached throughout the test were both potential failure loads. Given the first non-linearity, the failure load prediction was 1290 N, which was entirely agreed with almost 99% of the mean experimental failure load (1317.5 N). The numerical forecast (5800 N) agreed with the experimental data (17.9%) when the maximum load sustained during the test was used as the failure load. As mentioned before, the FRP-concrete

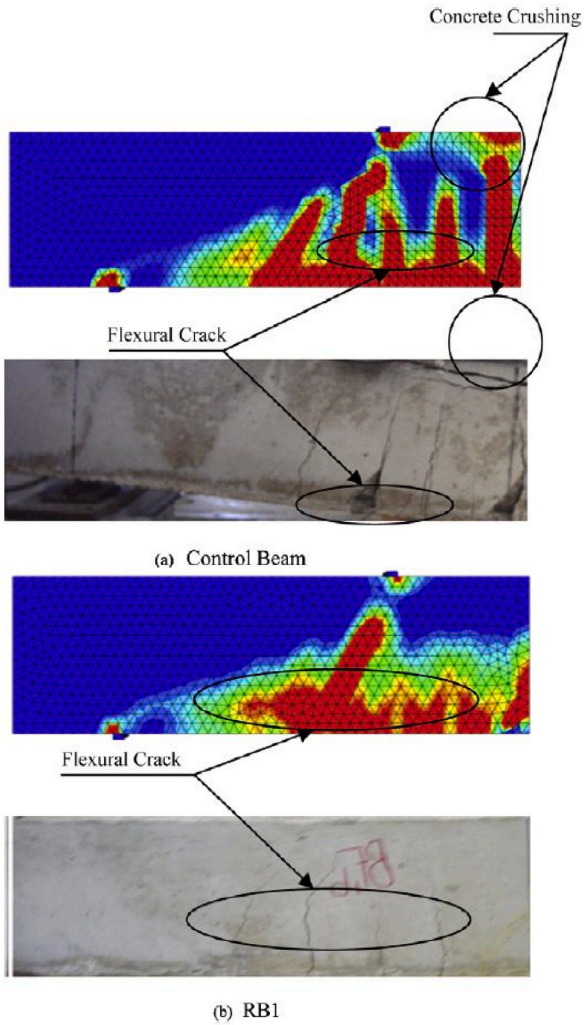

Fig. 33. Plastic strain distribution [40].

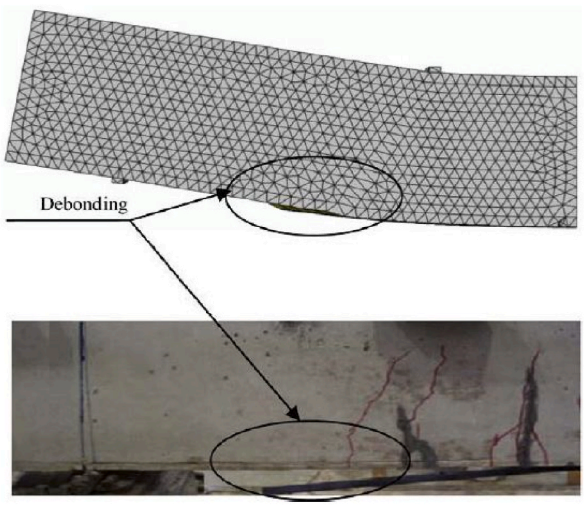

Fig. 34. Failure mode [40].

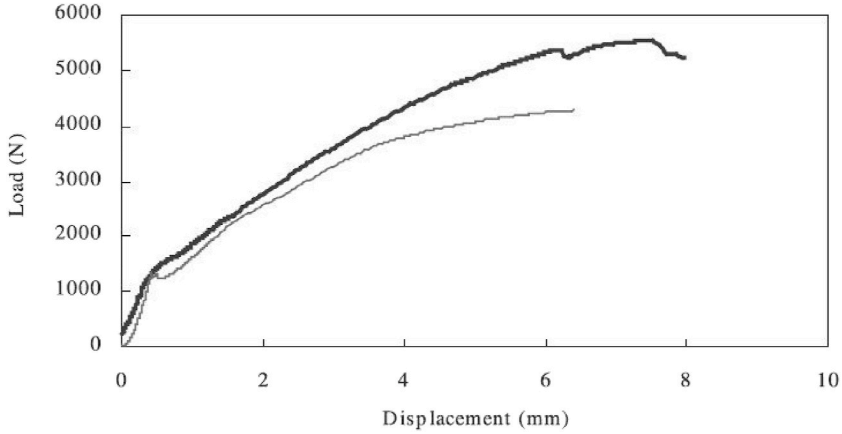

Fig. 35. Load-displacement (circular FRP) [41].

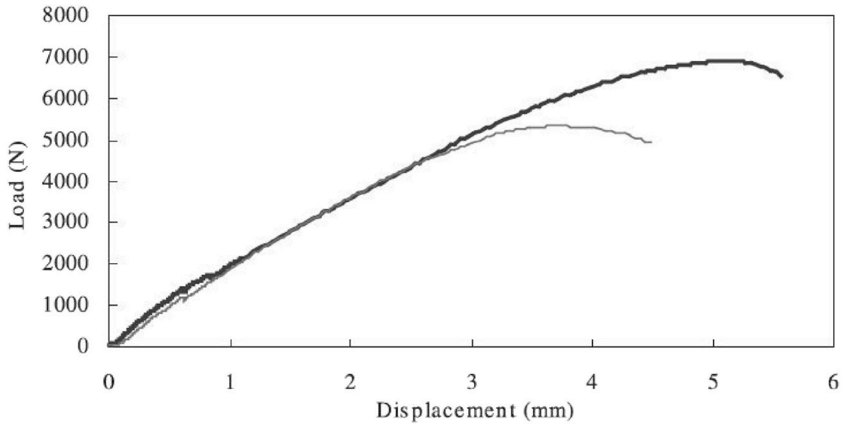

Fig. 36. Load-displacement (dog bone FRP) [41].

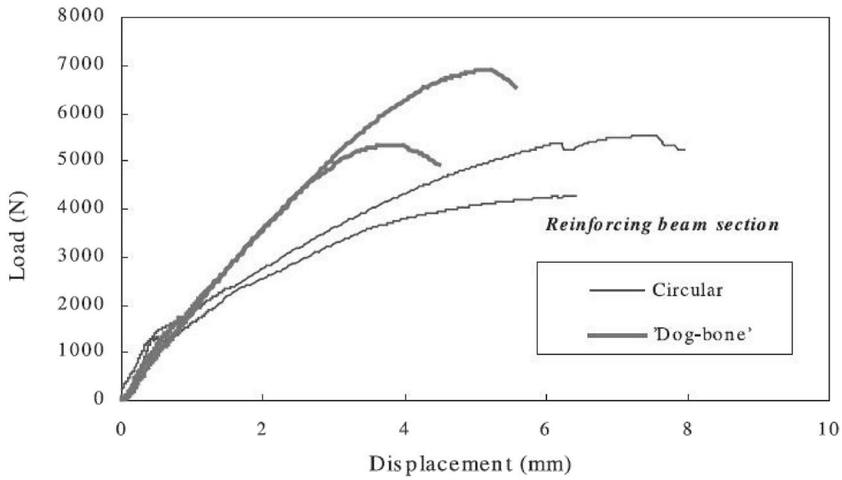

Fig. 37. Load-displacement (circular and dog-bone FRP) [41].

decohesion's effect contributed to this instance of overprediction of the failure load. Crushing of concrete on the contact zone with the loading roller affected the displacement values acquired using the cross-transducer heads. A transducer was thus attached to the underside of the specimen to provide a second displacement measurement independent of the computational prediction. The load-displacement relations were derived numerically for circular FRP reinforcements and compared to the acquired displacements obtained experimentally on the top and bottom faces of the specimen in Fig. 38. The stiffness reduction was primarily due to the widespread concrete cracking at large displacements, as seen in Fig. 38. The concrete crushing on the contact zone had little to no effects on the established results. The numerical model successfully predicted the material's initial (i.e., before cracking) stiffness and the initial non-linearity in the load-displacement relation. The forecasts were in reasonable agreement until a rough displacement of 2.5 mm. The numerical model overestimated the load borne by the beam when the displacement exceeded approximately 2.5 mm. The decohesion between the FRP rebar and the concrete beam might be blamed for this situation. FRP rebars were made via pultrusion manufacturing process with a relatively low coefficient of adhesion to concrete because of their flat surface. The computational model could not predict the decreased stiffness associated with this damage mechanism since decohesion was not considered.

4.3. (Yang et al., 2003) [42]

The numerical simulation demonstrated that the cracks gradually developed at the constant bending moment span for the un-plated beam and propagated to the shear span on the beam's tension surface. Within the continuous moment span, the crack spacing was approximately uniform, but in the shear span, it increased gradually towards the support. Some initial cracks remained intact, while other cracks eventually spread as the load increased. The cracked beam and the centre deflection of 7 mm at 100 kN stress are shown in Fig. 39(a) and Fig. 39(b). The displacement has been standardised to a scale of 50 for easier viewing. The rounded contours of the fissures seen in practice are accurately represented. This offered a substantial improvement as most earlier research required using pre-specified fracture routes. Table 17 demonstrates a close agreement between the predictions and the obtained test results for the beam.

The cracking process for the plated beam with a plate length of Lp = 2200 mm was remarkably similar to the unplated beam, with the exception that the cracks in the plated beam started at the concrete adhesive interface rather than at the beam's bottom surface. However, as seen in Fig. 40(a) and Fig. 40(b), the cracks in this beam are closed together and more evenly distributed compared to Fig. 39(a) and (b), respectively.

When the displacement parameter (d = 7 mm), as depicted in Fig. 40(c), the mesh for the plated beam shifted. As shown in Fig. 40 (b), the local stress concentration also caused a crack in the concrete near the end plate. In Fig. 39(a), the primary cracks in the unplated beam spread above the cross-section centre. However, they were still contained within the concrete cover for the plated beam, indicating that Ps = 100 kN was well within the allowable range, as depicted in Fig. 40(d). This suggested that the plate's bonding could greatly slow the crack propagation. It was important to remember that this study was conducted with monotonic loading, beginning with a beam free from stress and cracks. The preceding conclusion was only valid when the plate was bonded onto a beam that had never been loaded before. Pre-loading or cracking the beam could cause substantial variations. Since the plated beam reported in Ref. [24] had been loaded before being strengthened, this might address a large discrepancy between the test and projected values, as indicated in Table 1 when P = 100 kN. However, the difference induced by the various loading processes might diminish once the load exceeds the pre-loading level. The current prediction was consistent, showing high agreement with the experimental data for d = 7 mm.

At a stress of P = 334.1 kN, the primary tensile steel bar yielded, and the crack propagation analysis for the plated beam was continued. Fig. 41(d) delineates the cracked and deformed state of the beam at this point. Most first-seen fissures in Fig. 41(a) and (b) were extended and even fused to larger structures. The initial crack started at the plate's edge but only spread at a short distance. The beam failed in flexure. Nonetheless, a separate failure mode could be identified if the study was carried out past the first yielding of the major steel bars. The cracks occurred over the beam surface when the length of the FRP plate was shortened to Lp = 1600 mm, as depicted in Fig. 41. Many spaced cracks began early in the tension side of the reinforced part (Fig. 41(a)). At the stress between 105 and 111 kN, some cracks inside the constant bending moment span began to overgrow. The cracks began to show outside of the reinforced area (Fig. 41(b) and (c)). New cracks were opened in the continual bending moment between the larger ones. When the stress was Ps =

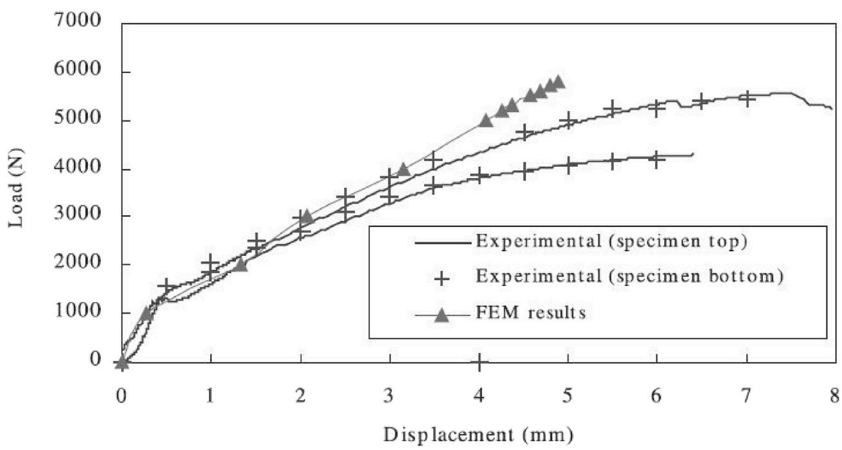

Fig. 38. Test results [41].

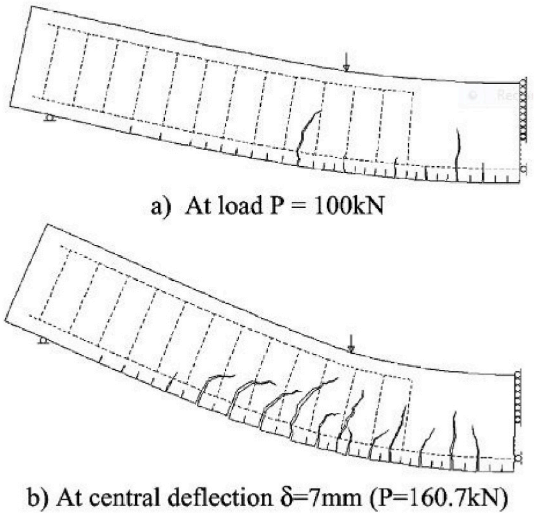

Fig. 39. Unplated beam [42].

Table 17
Predicted and test results [42].

Beam	Load (test/predicted) (kN), d = 7 mm	Central deflection (test/predicted) (mm), P = 100 kN
Unplated	160.0/160.7	3.98/3.55
Plated	173.0/188.6	3.74/2.54

141 kN, a nearly vertical crack occurred at the plate's edge. Some flexural fractures in the shear span near the loading point had spread out and cracked the longitudinal tension bars (Fig. 41(d)). Further stress increase caused several flexural fractures to propagate near the compression zone in the direction towards the loading point and caused flexural shear cracks to occur (Fig. 41(e)). The flexural crack that manifested at the plate's terminus grew to become the most extensive one. A fresh horizontal crack was started when this one met the tension steel reinforcement. This horizontal fissure, albeit visible, was still relatively small (Fig. 41(e)). Even though the primary fracture at the plate end was still widening at a certain load level, the horizontal crack quickly spread at the interface between the concrete cover and the tension steel reinforcements (Fig. 41(f)). The other cracks hardly altered after the horizontal fracture started to spread fastly. The beam failed as soon as this horizontal split joined up with the pre-existing large flexural shear crack (Fig. 41(g)). It was a fragile failure. The concrete cover separation failure was seen in many trials consistent with this projected failure mechanism.

4.4. (Sinaei et al., 2011) [43]

Five specimens (SC, S1, S2, S3, S4) had different shapes and lengths. Table 18 summarises the sample details used in this research. The theoretical rotation was determined from the change ratio of points A and B's vertical displacements to the change in their horizontal distance, as shown in Fig. 42. It was important to note that the distance between A and B was deliberately made large enough for all specimens to contain a plastic hinge zone.

Each specimen was tested for various characteristics, such as its ultimate load, concrete and reinforcement stress, FRP laminate stress, and ductility. The load-deflection curves for the control and reinforced specimens are delineated in Fig. 43, Fig. 44, Fig. 45, and Fig. 46. Table 19 and Fig. 47 also provide other findings, such as the joints' flexural capacities and the ductility factors for each specimen. Based on the experimental data results, a FEM was run to analyse and simulate the performance of FRP layers for exterior beam-column connections. A control specimen (non-retrofitted) and four retrofitted specimens with varying configurations of FRP were created to test the effects of retrofitting on the performance of beam-column joints in external RC. These tests aimed to determine how to enhance the lateral strength and ductility of the joints to boost their seismic performance. The options for connecting FRP to the beams' top, bottom, and lateral sides were considered for each specimen. The findings demonstrated that they were adequately designed, and the FRP composite could lead to respectable gains in ductility and strength. Non-linear analysis of realistic RC connections with FRP overlays confirmed the usefulness of L-shaped overlays made of FRP composite at the beam and column surface to improve ductility. Strong and flexible RC joints could be achieved by using U-shaped overlays beneath the beam and FRP on both lateral sides of the beam. However, the beam ductility was reduced when solely FRP was used on the top and bottom beam surfaces.

5. Numerical modelling

This section discusses general details of numerical modelling and steel and concrete materials modelling.

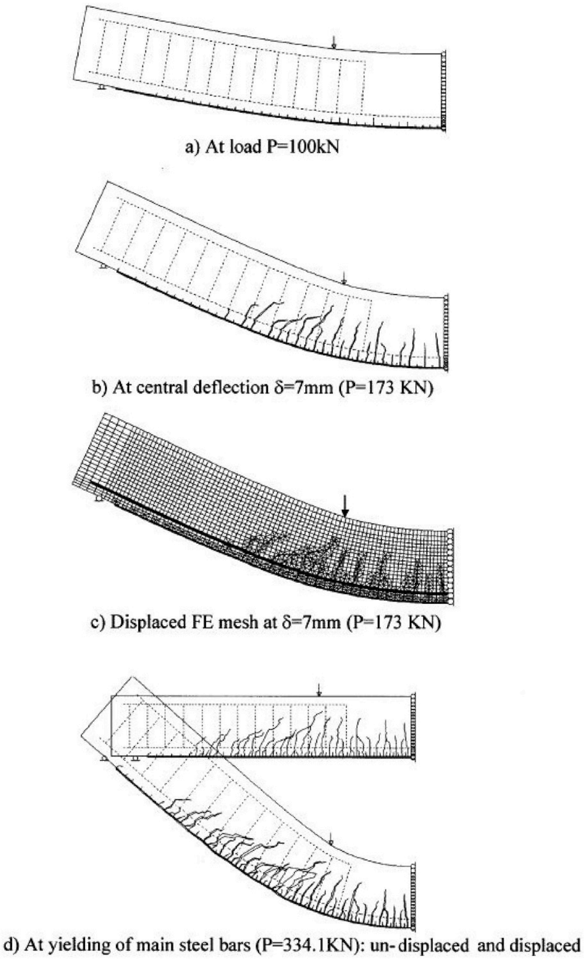

Fig. 40. Plated beam with Lp = 2200 mm [42].

5.1. General details

This numerical modelling of FRPRCB was constructed and analysed using the general FEA programme ABAQUS [44–47]. The structure members were modelled using a 4-node bilinear shell element (CPS4R) for concrete and strengthening members, including deviators and pins, and two 2-node linear truss elements (T2D2 and B21) for interior reinforcements. A 4-node bilinear shell element was used to model the concrete structural member. Moreover, 2-node linear truss elements (T2D2 and B21) were used for interior reinforcement. Deviators and pins also supported the FEM during the analysis running. This ABAQUS software is essential to use for getting the results. Based on the findings of the sensitivity analysis, a 20 mm mesh size was used. 20 mm is the optimum value to get the output results. This analysis of the theoretical section also used the same assumption called embedded command to get a simple modelling and concrete combination, including internal reinforcements. The links between the concrete beam and hole, saddle plate and anchor pin were produced using the surface-to-surface command. Since FRPRCB is mirror images of one another, it is only needed to model half of them to save time and computing power. As for contact interaction qualities, Lam et al. (2012) [48] considered the hard contact quality as common behaviour, and the 0.3 value was for the standard friction coefficient for tangential behaviour. This analysis was performed using only two-dimensional elements rather than the more time-consuming three-dimensional modelling that would have been required for the steel rod ends with bolt threads. The 'Equation' function merged the two joints instead of numerical modelling. Since thread failure was not the predominant mode of failure in this research, this simplification appeared appropriate. There were no analytical difficulties when the simulation began because there were no distances between the contact elements [49].

5.2. Steel modelling

The Equation functions (Eq. (1)) and (Eq. (2)) merged the two joints instead of doing detailed numerical modelling. Since thread failure was not the predominant mode of failure in this research, this simplification appeared appropriate.

$$\sigma_{true} = \sigma_{nom}\,(1+\varepsilon_{nom}) \tag{1}$$

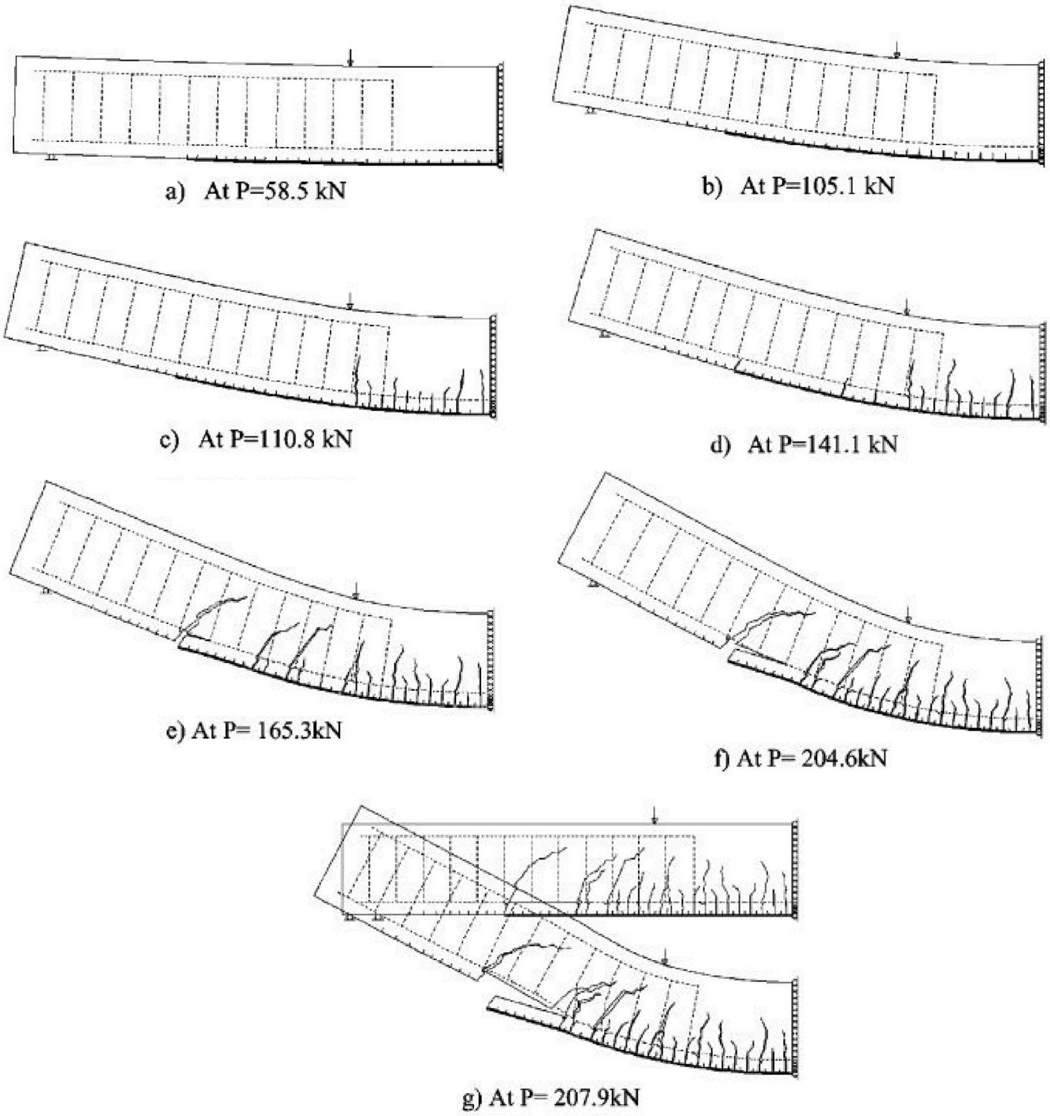

Fig. 41. Plated beam with Lp = 1600 mm [42].

Table 18
Specimen details [43].

Beam sample	Length (mm)
SC	–
S1	450 (Top and Bottom)
S2	450 (I-shape)
S3	750 (Both sides)
S4	450 (U-shape)

$$\varepsilon = \ln(1+\varepsilon_{nom}) - \sigma_{true}/E^{pl}_{ln} \quad (2)$$

where $\sigma true$ = true stress, $\varepsilon pl\ln$ = log strain, σnom = *nominal stress,* and εnom = nominal strain, E = Young's modulus. Based on the AIK, E = 200,000 MPa, and 205,000 MPa are the values utilised for reinforcement and external rods.

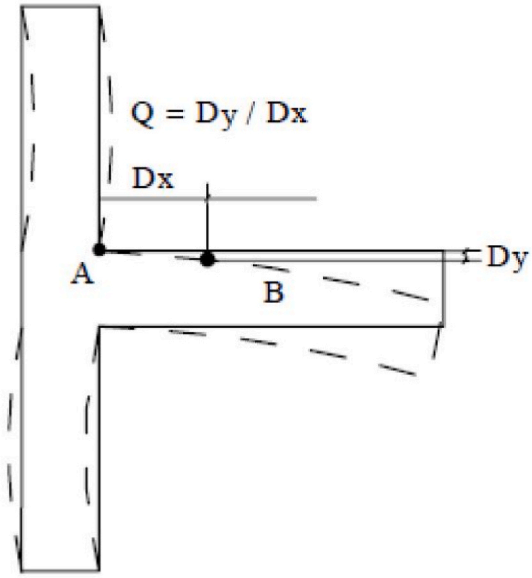

Fig. 42. Ductility determination [43].

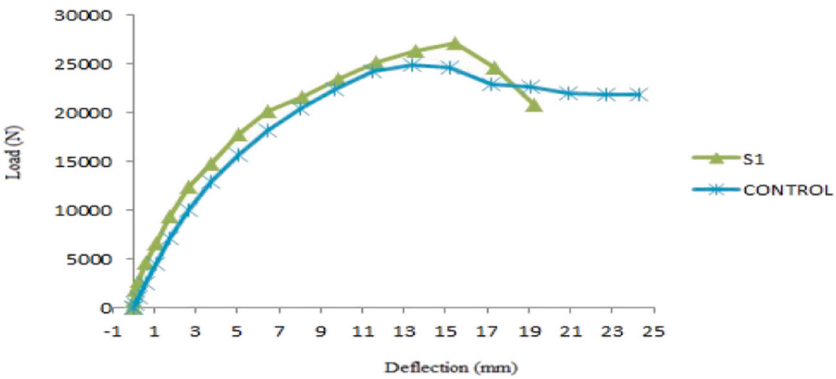

Fig. 43. Load-deflection [43].

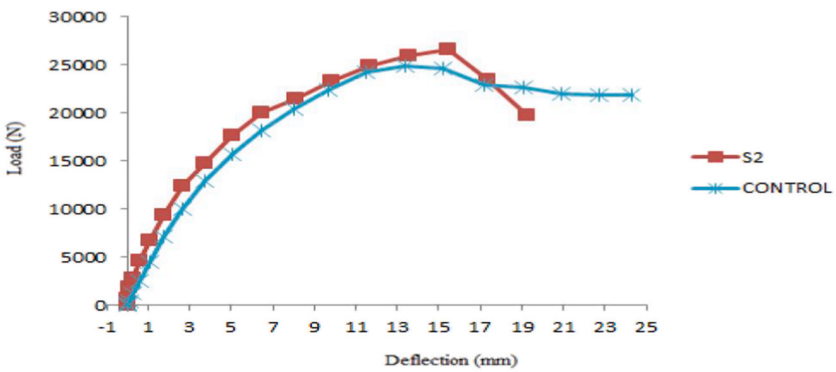

Fig. 44. Load-deflection [43].

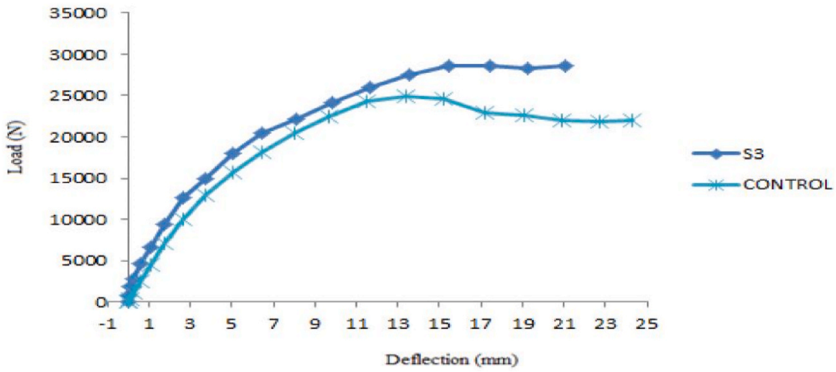

Fig. 45. Load-deflection [43].

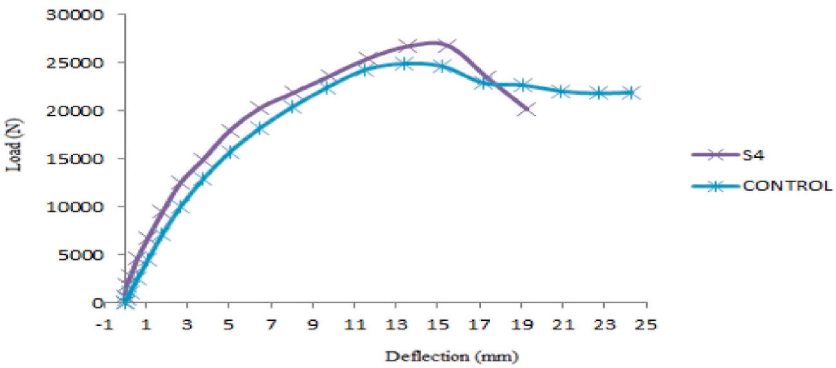

Fig. 46. Load-deflection [43].

Table 19
Ductility factor [43].

Beam sample	Maximum strength	Ductility
SC	24917	1.12
S1	27111	1.04
S2	26586	1.94
S3	28551	1.22
S4	26814	1.67

5.3. Concrete modelling

ABAQUS had a “Concrete Damaged Plasticity (CDP)” option that could be used to analyse the concrete damages. Some important parameters used in this investigation such as.

(1) Angle of dilation (ψ)
(2) Modulus of elasticity of concrete (Ec)
(3) Eccentricity (e)
(4) 1 direction of compression strength under biaxial loading to uniaxial compressive strength (fb0/fc0)
(5) Compression and tensile behaviour (S)
(6) Compressive meridian ratio (K)
(7) Viscosity (μ)

Ec = 4700 (f’c)0.5 MPa was defined as f’c from the compressive strength test, according to AIK (2016) [50] standards. This strength of compressive used a unit called MPa according to the ACI code [51]. Eccentricity (e) was set to 0.1. A compromise was reached between the formulas proposed by Papanikolaou and Kappos (2007) [52] and Tao et al. (2013) [53]: $fb_0/fc_0 = 1.5\ (fc_0)^{0.075}$. Based on the ACI code, $fc_0 = f'c$. It was not quantified in the experiments, and its data was rare in other studies. Based on a review of 14 scholarly sources, they devised their definition separately. The concrete yield surface was determined by the second stress invariant ratio on the

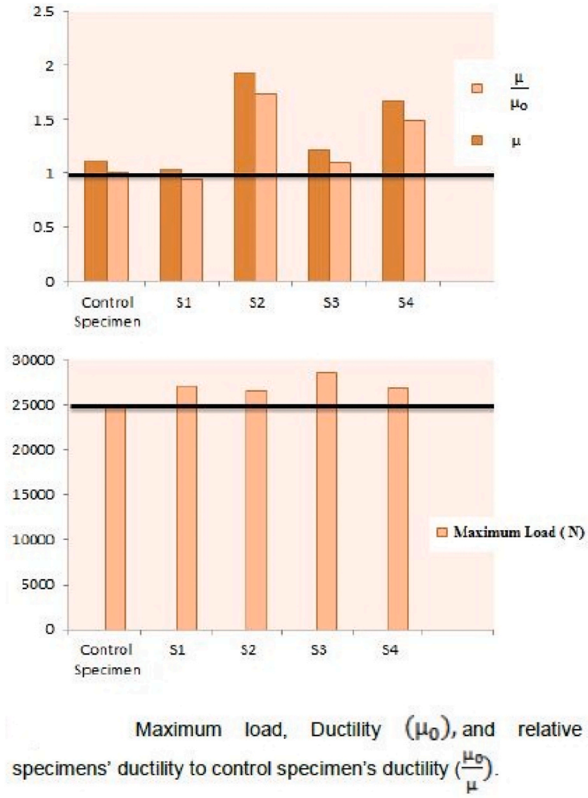

Fig. 47. Result details [43].

Table 20
Equation details.

Equations	References
Ec = 4700 (f'c)0.5 MPa	AIK (2016) [50]
$fb_0/fc_0 = 1.5\ (fc_0)^{0.075}$	Tao et al. (2013) [53]
K14 (5.5fb0)/(2f′$_c$5f$_{b0}$)	Yu et al. (2010) [55]

tensile meridian (K) to the compressive meridian (S). Many researchers, including Seow and Swaddiwudhipong (2005) [54], used 2/3 as a K default value, despite the K range being between 0.5 and 1.0. This research use Yu et al. (2010)'s [55] equation of K14 (5.5fb0)/(2f′$_c$5f$_{b0}$). Table 20 summarises all the equation details used.

ABAQUS had a range of 0° to 56° for defining the plastic flow potential [53]. This study relied heavily on the dilation angle (ψ) and viscosity parameter, even though previous studies found these challenging to quantify. Several researchers had used different values but had embraced them on a case-by-case basis. Numerous careful analyses led to 38° as an angle used in this study. Load-deflection behaviour was unaffected by its value, whereas plastic behaviour followed the elastic behaviour. The viscosity parameter (μ) was used in ABAQUS standard analysis for the visco-plastic regularisation of the concrete constitutive equation, and its default value was 0. 0 value was not useable because the numerical modelling did not advance into elastic behaviour. In comparison, Tao et al. (2013) [53] observed no influences on the parameter value's prediction accuracy.

The concrete compressive and tensile behaviour generally did not impact how the FRPRCB performed in terms of its structural performance. The following formula expressed compressive stress in concrete: f'c was the concrete's compressive strength, c_u was the ultimate compressive strain, and 0 was the maximum compressive strain. The stress-strain relationship was determined by Lou et al. (2013) [56] and Hognestad (2011) [57]. The tensile strength was achieved when the stress-strain increased consistently. The concrete tension curve was also required, and ABAQUS software was used to get the concrete tension curve (output) values by inserting the input values. The ABAQUS was run and analysed to get the output results. The higher the input values, the higher the output values. It was important to get excellent inputs to get the best output results. Here, the concrete used a tensile strength of 0.1f′c with 10ft/Ec ultimate tensile strain. The concrete properties were analysed with ABAQUS software. The damage in the specimen surpassed its tensile stress when the concrete fracture strain was exceeded [58–70]. Similar to what was found in the experiment, the FRPRCB under tensile stress had been deformed in ABAQUS simulation.

6. Investigated parameters on structural behaviour of fibre reinforced polymer reinforced concrete beams based on the experimental investigation and finite element analysis

Table 21 shows the different investigated parameters on the structural behaviour of FRP reinforced concrete beams. All these findings results are compared with each previously published researcher.

Table 21
Investigated parameters comparison.

References	Parameters	Experimental Test Types with Enhancement (e)/Reduction (r) Strength Compared to Control Specimen without FRP (%)		
		Load-deflection	Initial and post-cracking stiffness	Energy absorption for pre and post-cracking stages
	Opening			
(Chin et al., 2011) [27]	Circular	43 (e)	–	–
	Square	25.59 (r)	–	–
(Siew Choo Chin et al., 2015) [28]	Circular (No CFRP)	51 (r)	–	–
	Circular (Has CFRP)	56 (e)	–	–
	CFRP strengthening location			
(Laminates et al., 2014) [29]	Bottom	10 (e)	–	–
	Bottom (1/4 sides)	20 (e)	–	–
	Bottom (1/2 sides)	30 (e)	–	–
	Type and diameter of FRP bars			
(Karayannis et al., 2018) [31]	2HD5.5	–	3.88 (e)	–
	2HD10	–	1.93 (e)	–
	GFRP types			
(Narayanan, 2021) [32]	CM	50.57 (e)	–	74.01 (e)
	WR	56.29 (e)	–	117.32 (e)
	UD	5.18 (e)	–	29.40 (e)
	CSM + WR	64.48 (e)	–	118.90 (e)
	Steel stirrups			
(Venkatesha et al., 2013) [33]	6 mm@100 mm	5.11 (e)	–	–
	6 mm@120 mm	16.42 (e)	-	-
	6 mm@125 mm	18.11 (e)	–	–
	Bar type and shear reinforcement			
(Rahman et al., 2005) [34]	Austenitic SS bar (6 mm)	9.82 (r)	–	–
	FRP (3@16 mm) Stainless steel bar (6 mm)	16.39 (e)	–	–
	FRP (3@16 mm) SS mesh (3 mm diameter, 50 mm square opening)	54.92 (e)	–	–
	GFRP reinforcement type/ratio			
(Murugan & Kumaran, 2019) [35]	Sand coated/0.73	15 (r)	–	–
	Sand coated/1.08	5 (r)	–	–
	Threaded/0.73	25 (e)	–	–
	Threaded/1.08	40 (e)	–	–
	Thickness of GFRP bond layer			
(Yang, 2021) [36]	10 mm epoxy	221.05 (e)	98 (e)	–
	30 mm mortar	268.42 (e)	75 (e)	–
	30 mm mortar	294.74 (e)	62 (e)	–
	Reinforcement type			
(Bedon & Louter, 2019) [41]	Circular	21.57 (e)	–	–
	Dog-bone	24.39 (e)	–	–
	Beam types			
(Yang et al., 2003) [42]	Unplated	60 (e)	–	–
	Plated	73 (e)	–	–
	Beam shape/length (mm)			
(Sinaei et al., 2011) [43]	Top and bottom/450	8.81 (e)	–	–
	I shape/450	6.70 (e)	–	–
	U shape/450	14.58 (e)	–	–
	Both sides/750	7.61 (e)	–	–

7. Conclusion

The following primary conclusions are established based on the state-of-the-art review of various published experimental investigations and the FEA of FRPRCB.

7.1. Experimental investigation

1. The cracking around the opening is drastically reduced due to the strengthening arrangement of the FRP laminates at flexure. The beam deflection is reduced by about 61% compared to the case of a square opening. Even with the big circular opening, no appreciable lessening of beam deflection is seen. After being reinforced with FRP laminates, a beam with a wide circular opening in the middle span almost performs. In comparison, the flexural strength of the beam with a huge square aperture increases by 10%. Beams with big circular and square openings are 33% and 17% stiffer than unreinforced beams.
2. The behaviour of RC deep beams with large circular holes located in the shear region and strengthened by FRP wrap was investigated through experimental investigation. Shear failure, characterised by the formation of diagonal cracks at the top and bottom chords of the apertures, is shown to be the failure mode of deep beams with a large circular opening. The large circular opening in RC deep beam resulted in a significant loss of strength, with a 51% decrease in beam capacity compared to the control beam. The beam's maximum load capacity raises approximately 15.32% using surface strengthening via FRP wrap around the opening and only restores 56% of its original strength compared to the control beam.
3. Using FRP laminates to reinforce concrete beams decreases the beam deflection and boosts the load-carrying capacity. The cracks that didn't form are less severe and more widely spaced. Adding vertical layers of FRP can achieve additional load-carrying capacity and decrease deflection. Flexural strengthening fibres are less likely to break due to the presence of vertical layers.
4. Laying FRP debonding and decreasing corner stress concentration are the benefits of beam section alteration. The beam structural behaviour is greatly enhanced compared to its rectangular counterparts, but the required materials remain the same. Using FRP U-wraps is to get the most outstanding experimental results. When subjected to impact loading, RC beams that fail in flexure mode during static testing might fail in shear-flexure mode. The impact resistance should be designed using impact and inertial forces at the initial instant. The RCB must be locally strengthened in shear at the anticipated impact location to avoid shear failure. An anchor system should be implemented to protect RCB from early debonding caused by the impact stress. Finally, the testing results also show that FRP can be utilised to fortify RCB against impact load. Shear dominance and FRP debonding in impact tests are important considerations. The time lag between impact loads and reaction forces has also been analysed, as the early negative reaction forces are found.
5. The structural behaviour of FRP reinforced concrete beam shows more enhancements than reduction compared to control reinforced concrete beam without FRP based on the investigated parameters such as beam opening, FRP strengthening locations, types, diameters, thickness, reinforcement types and ratios. The FRP causes the load-deflection, initial and post-cracking stiffness, and energy absorption for pre and post-cracking stages of the reinforced concrete beam to increase and improve.

7.2. Finite element analysis

1. The length of the FRP has a significant impact on the performance of the retrofitted beams. Both experiments and FEA prove this. As the FRP is stretched out, the ultimate load increases. The cohesive model successfully models the bond behaviour between FRP and concrete. There was a strong correlation between experimental investigation and FEA for ultimate load, failure mode, and crack propagation.
2. Non-linearities in the materials and geometry were considered in the analysis of reinforced concrete reinforced with FRP. The concrete's model for compressive and tensile behaviour, as well as degradation to cracking and crushing, was investigated. The reinforcement made of composite material is viewed as elasto-brittle, whereas steel reinforcement is viewed as elasto-plastic. The concrete model's compressive behaviour was developed using strain-hardening plasticity method. A cut-off tension representation of a dual criterion for yielding and crushing in terms of stresses and strains was considered. The materials law for undirectional composite is linear elastic/brittle. Concrete can exhibit both elastic and flexible properties, as well as brittleness. This analysis focuses on a concrete beam reinforced with composite rebars but only has a single support. FRP rebars experimentally demonstrated the significance of the rebar geometry on the structural performance. In comparison to circular sections, the dog-bone produces a greater failure load, and more crack propagation occurs. Both experimental and FEA results concur very well.
3. The concrete cover separation failure mode in FRP-coated RC beams was successfully reproduced in FEA. The bonding of a plate resulted in smaller and more closely spaced cracks than the unreinforced beam, as shown by preliminary numerical data. The cracking can significantly impact the stress distribution of FRP plates used for plated beams. Before substantial cracks are formed or when the material is near its ultimate state, the stress distribution is uniform across the continuous bending moment span. The plate's length heavily influences the beam's failure mode. The FEA demonstrates that a beam strengthened with a short plate is more likely to fail due to concrete cover separation and in a more brittle manner than a beam strengthened with a long plate, assuming all other parameters remain identical.
4. The structural behaviour of FRP reinforced concrete beam shows more enhancements than reduction compared to control reinforced concrete beam without FRP based on the investigated parameters such as FRP reinforcement types, beam types, shapes and lengths. The FRP causes the load-deflection, initial and post-cracking stiffness, and energy absorption for pre and post-cracking stages of the reinforced concrete beam to increase and improve.

Author contribution statement

All authors listed have significantly contributed to the development and the writing of this article.

Funding statement

This research did not receive any specific grant from funding agencies in the public, commercial, or not-for-profit sectors.

Data availability statement

The data that has been used is confidential.

Declaration of interest's statement

The authors declare no conflict of interest.

References

[1] V. Rambabu, A.L. Naidu, S. Kona, Recent Advances in Material Sciences, 2019, pp. 17–26.
[2] K. Begum, M. Islam, Res. J. Eng. Sci. 2 (3) (2013) 46–53.
[3] F.I. Mahir, K.N. Keya, B. Sarker, K.M. Nahiun, R.A. Khan, Materials, Engineering Res. 1 (2) (2019) 86–97.
[4] H. Xu, X. Tong, Y. Zhang, Q. Li, W. Lu, Composites, Sci. Technol. 127 (2016) 113–118.
[5] A.S. Mosallam, A. Bayraktar, M. Elmikawi, S. Pul, S. Adanur, SOJ Mater. Sci. Eng 2 (2) (2015).
[6] I. Vrettos, E. Kefala, T.C. Triantaillou, ACI Struct. J. 110 (1) (2013).
[7] B.H. Osman, E. Wu, B. Ji, S.S. Abdulhameed, Int. J. Concrete Struct. Materials 11 (1) (2017) 171–183.
[8] A.A. Mohammed, A.C. Manalo, G.B. Maranan, M, Compos. Struct. 233 (2020), 111634.
[9] N. Aravind, A.K. Samanta, D.K. Roy, J.V. Thanikal, Curved And Layered Structures 1(open-Issue), 2015.
[10] J. Zhou, L. Wang, Sustainability 11 (4) (2019) 963.
[11] M. Haji, H. Naderpour, A. Kheyroddin, Compos. Struct. 209 (2019) 112–128.
[12] F. Peng, W. Xue, W. Xue, Database evaluation of shear strength of slender fiber-reinforced polymer-reinforced concrete members, ACI Struct. J. 117 (2020) 273–281, https://doi.org/10.14359/51723504.
[13] J.A.O. Barros, H. Baghi, A. Ventura-Gouveia, Assessing the applicability of a smeared crack approach for simulating the behaviour of concrete beams flexurally reinforced with GFRP bars and failing in shear, Eng. Struct. 227 (2021), 111391, https://doi.org/10.1016/j.engstruct.2020.111391.
[14] F. Peng, W. Xue, Design approach for flexural capacity of concrete T-beams with bonded prestressed and nonprestressed FRP reinforcements, Compos. Struct. 204 (2018) 333–341, https://doi.org/10.1016/j.compstruct.2018.07.091.
[15] C.W. Dolan, D. Swanson, Development of flexural capacity of a FRP prestressed beam with vertically distributed tendons, Compos. B Eng. 33 (1) (2002) 1–6.
[16] N. Grace, K. Ushijima, P. Baah, M. Bebawy, Flexural behavior of a carbon fiber-reinforced polymer prestressed decked bulb T-beam bridge system, J. Compos. Construct. 17 (4) (2013) 497–506, https://doi.org/10.1061/(ASCE)CC.1943- 5614.0000345.
[17] P. Nabipay, D. Svecova, Shear behavior of CFRP prestressed concrete T-beams, J. Compos. Construct. 18 (2) (2014), 04013049, https://doi.org/10.1061/(ASCE)CC.1943- 5614.0000450.
[18] Z. Wang, Y. Yao, D. Liu, Y. Cui, W. Liao, Shear behavior of concrete beams pre-stressed with carbon fiber reinforced polymer tendons, Adv. Mech. Eng. 11 (2019) 1–14.
[19] M. Nöel, K. Soudki, Effect of prestressing on the performance of GFRP-reinforced concrete slab bridge strips, J. Compos. Construct. 17 (2) (2013) 188–196.
[20] S.Y. Park, A.E. Naaman, Shear behavior of concrete beams prestressed with FRP tendons, PCI J. 44 (1) (1999) 74–85, https://doi.org/10.15554/pcij.01011999.74.85.
[21] N.F. Grace, S.B. Singh, M.M. Shinouda, S.S. Mathew, Concrete beams prestressed with CFRP, Concr. Int. 27 (2) (2005) 60–64.
[22] N.F. Grace, S.K. Rout, K. Ushijima, M. Bebawy, Performance of carbon-fiber-reinforced polymer stirrups in prestressed-decked bulb T-beams, J. Compos. Construct. 19 (3) (2015), 04014061, https://doi.org/10.1061/(ASCE)CC.1943-5614.0000524.
[23] S. Kueres, N. Will, J. Hegger, Shear strength of prestressed FRP reinforced concrete beams with shear reinforcement, Eng. Struct. 206 (2020), 110088.
[24] Z. Ma, M.K. Tadros, M. Baishya, Shear behavior of pretensioned high-strength concrete bridge I-girders, ACI Struct. J. 97 (2000) 185–192, https://doi.org/10.14359/848.
[25] F. Peng, W. Xue, Evaluation of Shear Design Provisions of Prestressed Concrete Beams with FRP Reinforcements. 6th Asia-Pacific Conference on FRP in Structures, 2017. Singapore.
[26] F. Castro, C. Vilarinho, D. Trancoso, P. Ferreira, F. Nunes, A. Miragaia, Utilisation of pulp and paper industry wastes as raw materials in cement clinker production, Int. J. Mater. Eng. Innovat. 1 (1) (2009) 74–90, https://doi.org/10.1504/IJMATEI.2009.024028.
[27] S.C. Chin, N. Shafiq, M.F. Nuruddin, Strengthening of RC Beams Containing Large Opening at Flexure with CFRP Laminates 5, 2011, pp. 743–749.
[28] Siew Choo Chin, F.M. Yahaya, D.O.H.S. Ing, A. Kusbiantoro, W.K. Chong, Experimental Study on Shear Strengthening of RC Deep Beams with Large Openings Using CFRP 1–7, 2015.
[29] F.R.P. Laminates, N.F. Grace, G.A. Sayed, A.K. Soliman, K.R. Saleh, Strengthening Reinforced Concrete Beams Using Fiber Reinforced Polymer (FRP) Laminates, 2014. September.
[30] T. Pham, H. Hao, Behavior of Fiber-Reinforced Reinforced Concrete Beams under Static and Impact Loads, 2016, https://doi.org/10.1177/2041419616658730. January 2019.
[31] C.G. Karayannis, P.K. Kosmidou, C.E. Chalioris, Bars — Experimental Study, 2018, https://doi.org/10.3390/fib6040099.
[32] P. Narayanan, Strength Behaviour of Fibre Reinforced Polymer Strengthened Beam STRENGTH BEHAVIOUR of FIBRE REINFORCED POLYMER, 2021. January 2006.
[33] K.V. Venkatesha, S.V. Dinesh, K. Balaji Rao, B.H. Bharatkumar, S.R. Balasubramanian, N.R. Iyer, Experimental investigation of reinforced concrete beams with and without CFRP wrapping, Slovak J. Civil Eng. 20 (3) (2013) 15–26, https://doi.org/10.2478/v10189-012-0014-7.
[34] A. Rahman, M. Sam, R.N. Swamy, Flexural behaviour of C oncrete beams reinforced with glass fibre reinforced polymer bars, Jurnal Kejuruteraan Awam 17 (1) (2005) 49–57.
[35] R. Murugan, G. Kumaran, Experiment on rc beams reinforced with glass fibre reinforced polymer reinforcements, Int. J. Innovative Technol. Explor. Eng. 8 (6 Special Issue 4) (2019) 35–41, https://doi.org/10.35940/ijitee.F1007.0486S419.
[36] J. Yang, Strengthening Reinforced Concrete Structures With FRP Composites Strengthening Reinforced Concrete Structures with FRP Composites Department of Architecture And Civil Engineering (Issue March), 2021, https://doi.org/10.13140/RG.2.2.15176.24325.

[37] A. Ahmed, M. Zillur Rahman, Y. Ou, S. Liu, B. Mobasher, S. Guo, D. Zhu, A review on the tensile behavior of fiber-reinforced polymer composites under varying strain rates and temperatures, Construct. Build. Mater. 294 (2021), 123565, https://doi.org/10.1016/j.conbuildmat.2021.123565.
[38] G. Muciaccia, M. Khorasani, D. Mostofinejad, Effect of different parameters on the performance of FRP anchors in combination with EBR-FRP strengthening systems: a review, Construct. Build. Mater. 354 (September) (2022), 129181, https://doi.org/10.1016/j.conbuildmat.2022.129181.
[39] M.Z. Naser, R.A. Hawileh, J.A. Abdalla, Fiber-reinforced polymer composites in strengthening reinforced concrete structures: a critical review, Eng. Struct. 198 (2019), 109542, https://doi.org/10.1016/j.engstruct.2019.109542.
[40] Y.T. Obaidat, Structural Retrofitting of Reinforced Concrete Beams Using Carbon Fibre Reinforced Polymer, 2022.
[41] C. Bedon, C. Louter, Structural glass beams with embedded GFRP, CFRP or steel reinforcement rods: comparative experimental, analytical and numerical investigations, J. Build. Eng. 22 (2019) 227–241, https://doi.org/10.1016/j.jobe.2018.12.008.
[42] Z.J. Yang, J. Chen, D. Proverbs, Finite Element Modelling of Concrete Cover Separation Failure in FRP Plated RC Beams, 2003, pp. 2–13, https://doi.org/10.1016/S0950-0618(02)00090-9, 0618(February).
[43] H. Sinaei, M.Z. Jumaat, M. Shariati, Numerical investigation on exterior reinforced concrete Beam-Column joint strengthened by composite fiber reinforced polymer, CFRP 6 (28) (2011) 6572–6579, https://doi.org/10.5897/IJPS11.1225.
[44] DS Simulia Corp, ABAQUS/CAE User's Guide, Dassault Systemes (DS) Simulia Corp., RI, USA, 2013.
[45] DS Simulia Corp, ABAQUS Analysis User's Guide, Dassault Systemes (DS) Simulia Corp., RI, USA, 2013.
[46] DS Simulia Corp, ABAQUS Example Problems Guide, Dassault Systemes (DS) Simulia Corp., RI, USA, 2013.
[47] DS Simulia Corp, ABAQUS Theory Guide, Dassault Systemes (DS) Simulia Corp., RI, USA, 2013.
[48] D. Lam, X.H. Dai, L.H. Han, Q.X. Ren, W. Li, Behaviour of inclined, tapered and STS square CFST stub columns subjected to axial load, Thin-Walled Struct. 54 (2012) 94–105.
[49] X.H. Dai, Y.C. Wang, C.G. Bailey, Numerical modelling of structural fire behaviour of restrained steel beam-column assemblies using typical joints types, Eng. Struct. 32 (8) (2010) 2337–2351.
[50] AIK, Korean Building Code and Commentary (KBC 2016), Architectural Institute of Korea (AIK), Seoul, Korea, 2016 (in Korea).
[51] ACI 318 Committee, Building Code Requirements for Structural Concrete (ACI 318- 14) and Commentary (ACI 318R-14), American Concrete Institute (ACI), Farmington Hills, MI, USA, 2014.
[52] V.K. Papanikolaou, A.J. Kappos, Confinement-sensitive plasticity constitutive model for concrete in triaxial compression, Int. J. Solid Struct. 44 (21) (2007) 7021–7048.
[53] Z. Tao, Z.B. Wang, Q. Yu, Finite element modelling of concrete-filled steel stub columns under axial compression, J. Constr. Steel Res. 89 (2013) 121–131.
[54] P.E.C. Seow, S. Swaddiwudhipong, Failure surface for concrete under multiaxial load – a unified approach, J. Mater. Civ. Eng. 17 (2) (2005) 219–228.
[55] T. Yu, J.G. Teng, Y.L. Wong, S.L. Dong, Finite element modeling of confined concrete I: drucker-Prager type plasticity model, Eng. Struct. 32 (3) (2010) 665–679.
[56] T. Lou, S.M.R. Lopes, A.V. Lopes, Flexural response of continuous concrete beams prestressed with external tendons, J. Bridge Eng. 18 (6) (2013) 525–537.
[57] E. Hognestad, A Study of Combined Bending and Axial Load in Reinforced Concrete Members, University of Illinois Engineering Experimental Station, IL, USA, 2011.
[58] Bin Azuwa Solahuddin, The Effect of Shredded Paper As Partial Sand Replacement on Properties of Cement Sand Brick. Bachelor's Degree Thesis, Universiti Malaysia Pahang, 2017.
[59] B.A. Solahuddin, F.M. Yahaya, Effect of shredded waste paper on properties of concrete, IOP Conf. Ser. Mater. Sci. Eng. 1092 (1) (2021), 012063, https://doi.org/10.1088/1757-899x/1092/1/012063.
[60] B.A. Solahuddin, F.M. Yahaya, Load-strain behaviour of shredded waste paper reinforced concrete beam, IOP Conf. Ser. Mater. Sci. Eng. 1092 (1) (2021), 012063, https://doi.org/10.1088/1757-899x/1092/1/012063.
[61] B.A. Solahuddin, F.M. Yahaya, A review paper on the effect of waste paper on mechanical properties of concrete, IOP Conf. Ser. Mater. Sci. Eng. 1092 (1) (2021), 012063, https://doi.org/10.1088/1757-899x/1092/1/012067.
[62] B.A. Solahuddin, F.M. Yahaya, Structural behaviour of shredded waste paper reinforced concrete beam, Int. J. Adv. Res. Eng. Innovation 3 (1) (2021) 74–87. https://myjms.mohe.gov.my/index.php/ijarei/article/view/12968.
[63] B.A. Solahuddin, F.M. Yahaya, Inclusion of Waste Paper on Concrete Properties: A Review, Civil Engineering Journal-Tehran, 2021, pp. 94–113, https://doi.org/10.28991/CEJ-SP2021-07-07, 7(Special Issue-Innovative Strategies in Civil Engineering Grand Challenges).
[64] B.A. Solahuddin, A critical review on experimental investigation and finite element analysis on structural performance of kenaf fibre reinforced concrete, Structures 35 (November 2021) (2022) 1030–1061, https://doi.org/10.1016/j.istruc.2021.11.056.
[65] B.A. Solahuddin, F.M. Yahaya, Properties of concrete containing shredded waste paper as an additive, Mater. Today Proc. 51 (2022) 1350–1354, https://doi.org/10.1016/j.matpr.2021.11.390.
[66] B.A. Solahuddin, A review on structural performance of bamboo reinforced concrete, Mater. Sci. Forum 1056 (2022) 75–80, https://doi.org/10.4028/p-dx1x87. MSF.
[67] B.A. Solahuddin, Strengthening of reinforced concrete with steel fibre: a review, Mater. Sci. Forum 1056 (2022) 81–86, https://doi.org/10.4028/p-3g0h57.
[68] B.A. Solahuddin, A review on the effect of reinforcement on reinforced concrete beam-column joint behavior, in: Proceedings of Malaysian Technical Universities Conference on Engineering and Technology (MUCET) 2021, 2022.
[69] B.A. Solahuddin, Seismic performance of reinforced concrete beam-column joint: a review, in: Proceedings of Malaysian Technical Universities Conference on Engineering and Technology (MUCET) 2021, 2022.
[70] B.A. Solahuddin, A comprehensive review on waste paper concrete, Res. Eng. 16 (October) (2022), 100740, https://doi.org/10.1016/j.rineng.2022.100740.